Advances in Materials Science and Engineering

Innovative Materials in Safety Systems Design and Manufacturing

Lead Guest Editor: Lucian-Ionel Cioca
Guest Editors: Radian Belu, Aron Gabor, and Costica Bejinariu

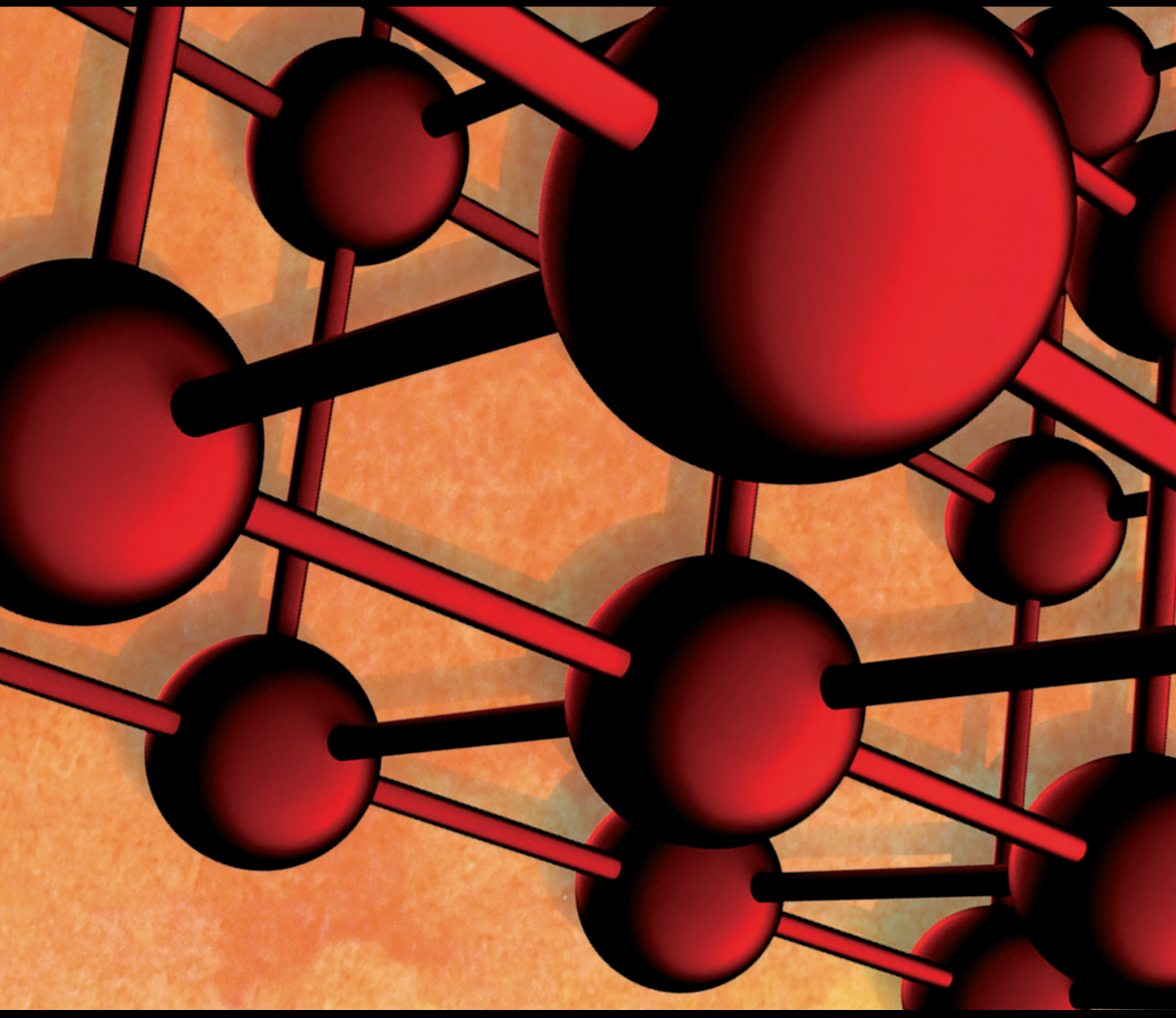

Innovative Materials in Safety Systems Design and Manufacturing

Advances in Materials Science and Engineering

Innovative Materials in Safety Systems Design and Manufacturing

Lead Guest Editor: Lucian-Ionel Cioca
Guest Editors: Radian Belu, Aron Gabor, and Costica Bejinariu

Contents

Hindawi
Advances in Materials Science and Engineering
Volume 2020, Article ID 9260818, 12 pages
https://doi.org/10.1155/2020/9260818

Research Article

Kinetic Analysis of the Thermal Decomposition of Polymer-Bonded Explosive Based on PETN: Model-Fitting Method and Isoconversional Method

Trung Toan Nguyen,[1] Duc Nhan Phan,[1] Van Thom Do,[2] and Hoang Nam Nguyen[3]

[1]*Faculty of Special Equipment, Le Quy Don Technical University, 236 Hoang Quoc Viet, Ha Noi 100000, Vietnam*
[2]*Faculty of Mechanical Engineering, Le Quy Don Technical University, 236 Hoang Quoc Viet, Hanoi 100000, Vietnam*
[3]*Modeling Evolutionary Algorithms Simulation and Artificial Intelligence, Faculty of Electrical & Electronics Engineering, Ton Duc Thang University, Ho Chi Minh City, Vietnam*

Correspondence should be addressed to Hoang Nam Nguyen; nguyenhoangnam@tdtu.edu.vn

Received 25 August 2019; Revised 30 May 2020; Accepted 17 June 2020; Published 11 July 2020

Academic Editor: Alain Portavoce

This work investigates kinetics and thermal decomposition behaviors of pentaerythritol tetranitrate (PETN) and two polymer-bonded explosive (PBX) samples created from PETN (named as PBX-PN-85 and PBX-PP-85) using the vacuum stability test (VST) and thermogravimetry (TG/DTG) techniques. Both model-free (isoconversional) and model-fitting methods were applied to determine the kinetic parameters of the thermal decomposition. It was found that kinetic parameters obtained by the modified Kissinger–Akahira–Sunose method (using non-isothermal TG/DTG data) were close to those obtained by the isoconversional and model-fitting methods that use isothermal VST data. The activation energy values of thermal decomposition reactions were 125.6–137.1, 137.3–144.9, and 143.9–152.4 kJ·mol^{-1} for PBX-PN-85, PETN, and PBX-PP-85, respectively. The results demonstrate the negative effect of the nitrocellulose-based binder in reducing the thermal stability of single PETN, while the polystyrene-based binder seemingly shows no adverse influence on the thermal decomposition of PETN in our presented PBX compositions.

1. Introduction

Pentaerythritol tetranitrate (also called PETN), which is a popular nitrate explosive, is extensively used in civilian and military applications due to its high energy characteristics [1, 2]. The main drawback of PETN is that it is highly sensitive to impact and friction pulses, and thus there may be explosion risks in the processes of production, storage, and especially in the transportation of PETN. Therefore, PETN is often used in the form of a polymer-bonded explosive (also called PBX) [3–5] to overcome this shortcoming. The PBX sample based on PETN is a composite explosive in which the PETN particles are covered and bonded by the polymeric binder. The polymeric binder in PBX composition can reduce the sensitivity of explosive to mechanical pulses and make the charge compression easier and safer [6–9].

Like all other high-energy materials, the PBX composition is also an unstable thermodynamic system [10]. Compared to the single explosive such as PETN, the thermal decomposition of PBX is generally more complex because of the incompatible reactions between explosives and the polymeric binders [11–14], and the safety and performance of PBX sample may change during aging. Therefore, the behaviors and kinetics of thermal decomposition of PBX samples should be evaluated and clarified to assess the safety and the thermal hazard potential during storage. The decomposition kinetics and thermal behaviors of several composite explosives based on PETN have been carefully examined, and it was shown that the presence of the additive materials exerts powerful impacts on the thermal decomposition of these explosives [15–19].

In this study, we investigate the thermal decomposition kinetics of two PETN-based PBX samples named as PBX-PN-85 and PBX-PP-85. These results were compared with those of a single PETN to evaluate the influence of binders on the thermal decomposition behaviors of explosives. Thermal analyses were conducted by thermogravimetry (TG/DTG) and vacuum stability test (VST), where the VST method (developed by STABIL, Czech Republic) is commonly used to examine the chemical stability, compatibility, and shelf-life of energetic materials in recent years [10, 14, 20]. Based on TG/DTG curves and VST results, we determined kinetic parameters by using isoconversional and model-fitting methods according to the ICTAC kinetics committee recommendations [21]. It is noteworthy that while model-fitting and isoconversional methods are both applicable to isothermal data, the model-fitting method is generally not applicable to non-isothermal techniques since the kinetic parameters obtained for non-isothermal data utilizing model-fitting technique are highly variable [22].

2. Materials and Methods

2.1. Materials. We imported Class-1 PETN with a melting temperature of over 139.0°C from South Korea. Good quality nitrocellulose (NC), that has a nitrogen content of 12.20%, was supplied from the Vietnam factory. Polystyrene (PS), which has an average molecular weight of 80,000 u, was produced in our laboratory. The widely used plasticizer, dioctyl phthalate (DOP), was utilized to make the binder from the PS and NC (the ratios of DOP/NC and DOP/PS were 3/1 and 2/1, respectively). Besides, some suitable solvents such as toluene and ethyl acetate are used in this study.

2.2. Experimental Techniques and Methods

2.2.1. Preparation of PBX Samples. PS and NC were plasticized by DOP (the ratios of DOP/NC and DOP/PS are 3/1 and 2/1, respectively), then dissolved in the suitable solvents (toluene for PS and ethyl acetate for NC), maintaining the polymer/solvent ratio of 1/15 (w/v), and kept for approximately 5 hours to obtain a homogeneous solution. The sample preparation method was carried out by mixing PETN crystals with the binders based on PS and NC. The mixing process took place on the heating device at 70°C for 30 minutes, and the PETN crystals were covered by the binder layers [6, 23]. After that, the mixtures were vacuum-dried at 60 to 70°C for 5 hours to remove the solvents. Table 1 shows the compositions of two proposed PBX samples.

2.2.2. Experimental Techniques. The thermal decomposition behaviors of PBX samples were determined by employing thermogravimetry (TG/DTG) and vacuum stability test (VST). The experimental conditions are as follows.

TG/DTG analysis was conducted using a NETZSCH STA 409 PC/PG (NETZSCH-Gerätebau GmbH, Selb, Germany). PBX samples (around 5.0 mg) were put in an aluminum oxide crucible and heated at various heating rates of 3, 5, 7, and 10 K·min^{-1}. The sample vial was heated from 30 to 350°C. Experimental heating processes were carried on under a dynamic nitrogen atmosphere with a flow rate of 30 mL·min^{-1}.

Table 1: The composition of two PBX samples based on PETN.

Composition	Content of materials (wt%)			
	PETN	DOP	PS	NC
PBX-PP	85.00	10.00	5.00	—
PBX-PN	85.00	11.25	—	3.75

The VST test was carried out in a STABIL apparatus (OZM Research, Pardubice, Czech Republic). During this test, PBX samples were heated isothermally at different temperatures of 135, 140, 145, and 150°C under vacuum pressure (at most 0.672 kPa). A pressure sensor and a computer are used to record the relationship of the released gas volume versus heating time. The sample mass was 20.0 mg, and we performed the test from 5 to 10 days (depending on the temperature test), until the end of the thermal decomposition reaction.

2.2.3. Kinetics Analysis. The kinetics of thermal decomposition reactions in solids can be expressed as the following equation:

$$\frac{d\varphi}{dt} = k(T) \cdot c(\varphi), \tag{1}$$

where t is time (s); φ is the extent of conversion; T is the temperature (K); and $k(T)$ is a function of conversion representing the reaction model. For the TG tests, the extent of conversion φ is defined as follows:

$$\varphi_t = \frac{m_i - m_t}{m_i - m_f}, \tag{2}$$

where m_i, m_t, and m_f are the initial sample mass, sample mass at any time t, and sample mass at the end of the decomposition, respectively. For the VST test, the value of φ is expressed as [13, 24]

$$\varphi_t = \frac{p_t - p_0}{p_{\max} - p_0}, \tag{3}$$

where $p_{\max}$ is the pressure at the end of decomposition, p_t is the pressure at any time t, and p_0 is initial pressure. Following the Arrhenius equation, $k(T)$ is computed by

$$k(T) = A \cdot e^{-E/\mathrm{RT}}, \tag{4}$$

where R, T, E, and A are the universal gas constant, absolute temperature, activation energy, and pre-exponential factor, respectively.

(1) Model-Fitting Method. Model-fitting methods employed different forms of reaction model for finding the referred decomposition kinetic parameters; some of these reaction models are illustrated in Table 2.

For isothermal conditions, equation (1) can be used in the integral form as follows [22, 24]:

Table 2: Different reaction models generally applied to describe the thermal decomposition in solids [21, 22, 24, 25].

Model no.	Reaction model	$c(\varphi)$	$i(\varphi)$
1	Avarami-Erofe'ev (A2)	$2(1-\varphi)[-\ln(1-\varphi)]^{1/2}$	$[-\ln(1-\varphi)]^{1/2}$
2	Avarami-Erofe'ev (A3)	$3(1-\varphi)[-\ln(1-\varphi)]^{2/3}$	$[-\ln(1-\varphi)]^{1/3}$
3	Avarami-Erofe'ev (A4)	$4(1-\varphi)[-\ln(1-\varphi)]^{3/4}$	$[-\ln(1-\varphi)]^{1/4}$
4	Power law (P2)	$2\varphi^{(1/2)}$	$\varphi^{(1/2)}$
5	Power law (P3)	$3\varphi^{(2/3)}$	$\varphi^{(1/3)}$
6	Power law (P4)	$4\varphi^{(3/4)}$	$\varphi^{(1/4)}$
7	1-D diffusion (D1)	$1/(2\varphi)$	φ^2
8	2-D diffusion (D2)	$[-\ln(1-\varphi)]^{-1}$	$[(1-\varphi)\ln(1-\varphi)]+\varphi$
9	3-D diffusion-Jander (D3)	$[3(1-\varphi)^{2/3}]/2[1-(1-\varphi)^{1/3}]$	$[1-(1-\varphi)^{1/3}]^2$
10	First-order (F1)	$(1-\varphi)$	$-\ln(1-\varphi)$
11	Second-order (F2)	$(1-\varphi)^2$	$(1-\varphi)^{-1}-1$
12	Third-order (F3)	$(1-\varphi)^3$	$[(1-\varphi)^{-2}-1]/2$
13	Contracting area (R2)	$2(1-\varphi)^{1/2}$	$[1-(1-\varphi)^{1/2}]$
14	Contracting volume (R3)	$3(1-\varphi)^{2/3}$	$[1-(1-\varphi)^{1/3}]$

$$i(\varphi)=\int_0^{\varphi}[c(\varphi)]^{-1}\mathrm{d}\varphi=k(T)t, \tag{5}$$

where $i(\varphi)$ is the integrated form of the reaction model $c(\varphi)$. Replacing each reaction model from Table 1 into equation (5), the rate constant can be computed from the slope of the straight line when plotting $i(\varphi)$ against t. Then, we can base on $i(\varphi)$ and $c(\varphi)$ formulations in the reaction model to determine $k(T)$. For each selected reaction model, $k(T)$ is determined at different temperatures, and the kinetic parameters can be calculated by the Arrhenius equation:

$$\ln k(T)=\ln A-\left(\frac{E}{RT}\right). \tag{6}$$

(2) Isoconversional (Model-Free) Method. The reaction model (as in equation (1)) in the isoconversional method is considered as being independent of temperature. Under the isothermal condition of the VST test, combining equations (4) and (5), we obtain [13, 22, 24]

$$-\ln t_{\varphi,j}=\ln\left[\frac{A}{i(\varphi)}\right]-\frac{E_\varphi}{RT_j}, \tag{7}$$

where the activation energy (E_φ) is estimated from the slope of the straight line when plotting ($-\ln t_{\varphi,j}$) against ($1/T_j$). Thus, the dependencies of activation energy (E_φ) on the conversion of the thermal decomposition (φ) could be obtained.

At a linear heating rate $\beta=\mathrm{d}T/\mathrm{d}t$ and under non-isothermal condition, equation (1) can be described as the following:

$$\frac{\mathrm{d}\varphi}{\mathrm{d}t}=\beta\frac{\mathrm{d}\varphi}{\mathrm{d}T}=Ae^{-E/RT}c(\varphi), \tag{8}$$

and Kissinger, Akahira, and Sunose introduced the model-free method using the following linear equation [22, 26]:

$$\ln\left(\frac{\beta_k}{T^2_{\varphi,k}}\right)=\ln\left(\frac{AR}{i(\varphi)E_\varphi}\right)-\frac{E_\varphi}{RT_\varphi}. \tag{9}$$

For each extent of conversion φ, the values of E and A can be found from the slope and the intercept when plotting $\ln(\beta/T^2)$ against $1/T$. The function $i(\varphi)$ can be determined according to the methodology reported in the literature [27, 28].

3. Results and Discussions

3.1. The TG/DTG Results. TG/DTG curves of PETN, PBX-PN-85, and PBX-PP-85 at different heating rates (i.e., 3, 5, 7, and 10 K·min^{-1}) were recorded and are shown in Figure 1.

For comparison, the characteristic parameters of TG/DTG curves of PETN, PBX-PN-85, and PBX-PP-85 are summarized in Table 3.

It has been shown that only a single decomposition step is related to the thermal decomposition of a single PETN (i.e., one-step reaction model) in all samples. The peak temperatures in DTG curves for the thermal decomposition of PETN, PBX-PN-85, and PBX-PP-85 were observed in a range of 186–201, 183–199, and 189–204°C, respectively. Generally, the decomposition residue of all samples increases with the increasing heating rate, and the residue mass of PBX-PN-85 and PBX-PP-85 may be less than that of PETN because of the presence of inert ingredient (i.e., DOP and PS) in their formulation.

As seen, the thermal decomposition of PETN occurred at a higher temperature than PBX-PN-85 but lower than that of PBX-PP-85. DTG curves in Figure 1 also demonstrated the role of the binder on the thermal decomposition behaviors of PETN. Thermal stability and decomposition temperature of single PETN are clearly affected by the binders. Specifically, the energetic binder (i.e., NC-based binder) reduces the decomposition temperature of single PETN, while the nonenergetic binder (i.e., PS-based binder) hardly affects the thermal stability of PETN. Interestingly, the PBX-PN-85 sample also shows an early decomposition. This may be caused by the exothermic decomposition effect of NC and the release of the gaseous products in the early decomposition of PETN in the binder matrix [13]. Contrarily, the decomposition temperature of PBX-PP-85 has a slight increase because this PBX sample has less amount of PETN (compared to single PETN) in its composition [8].

According to equation (2), the corresponding curve of the conversion φ versus temperature T was obtained and is

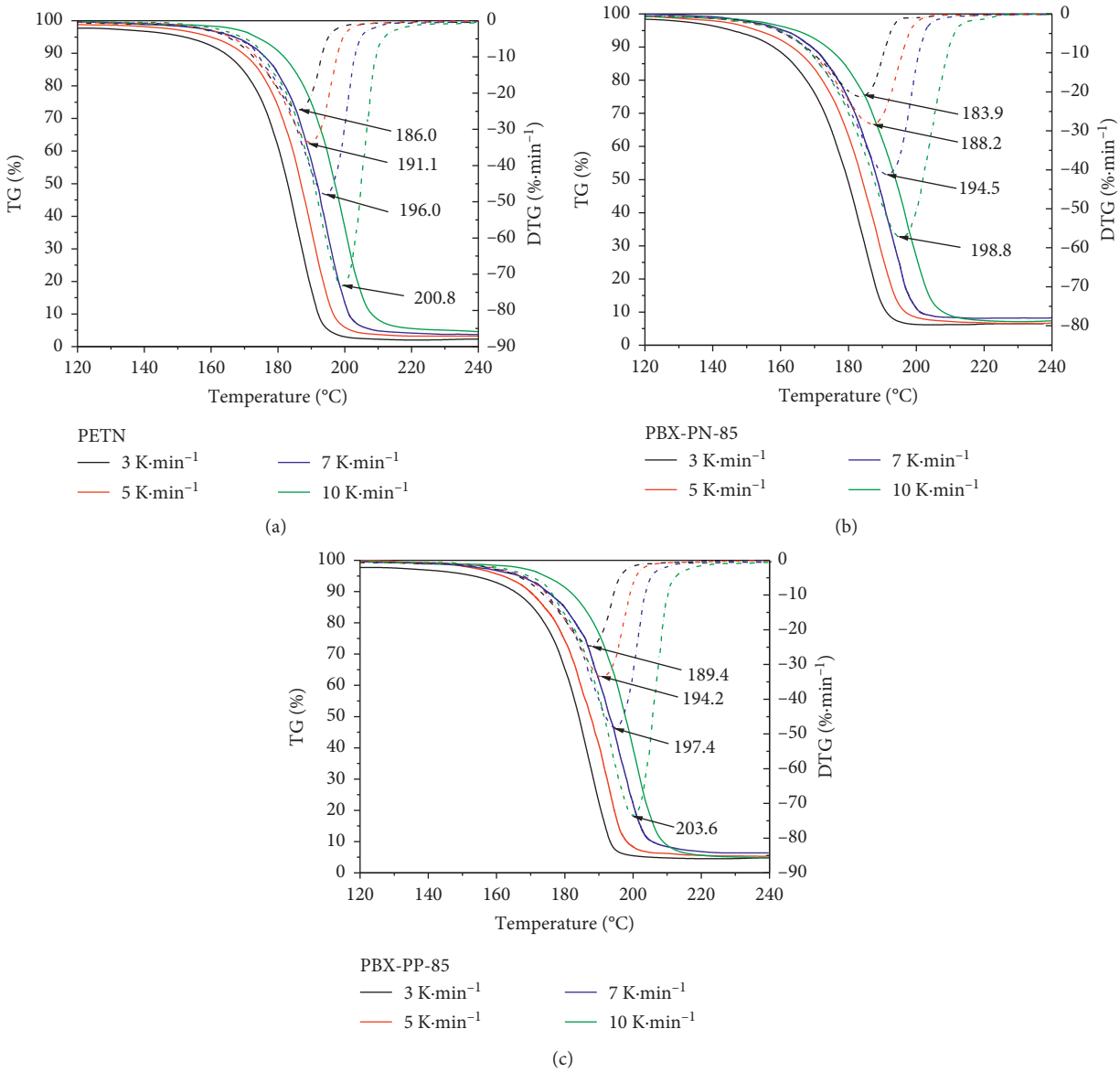

Figure 1: TG/DTG curves of PETN, PBX-PN-85, and PBX-PP-85 at several heating rates.

Table 3: Kinetic parameters from TG/DTG data of PBX-PN-85, PBX-PP-85, and PETN.

Material	β (K·min^{-1})	TG/DTG curve				
		T_{ot} (°C)	T_i (°C)	T_p (°C)	Mass loss (%)	Residue (%)
PETN	3.0	165.5	130.2	186.0	98.3	1.7
	5.0	169.6	132.0	191.1	97.2	2.8
	7.0	172.7	133.2	196.0	96.3	3.7
	10.0	178.9	135.6	200.8	96.0	4.0
PBX-PN-85	3.0	162.3	127.1	183.9	95.3	4.7
	5.0	166.8	129.8	188.2	94.4	5.6
	7.0	169.0	130.9	194.5	94.0	6.0
	10.0	175.3	133.5	198.8	93.1	6.9
PBX-PP-85	3.0	168.6	136.2	189.4	93.7	6.3
	5.0	172.5	138.0	194.2	93.1	6.9
	7.0	177.0	139.9	197.4	91.5	8.5
	10.0	183.2	142.5	203.6	91.9	8.1

T_{ot}—onset temperature of decomposition exotherm peak, T_i—the initial temperature of the mass loss, and T_p—the peak temperature of the DTG curve.

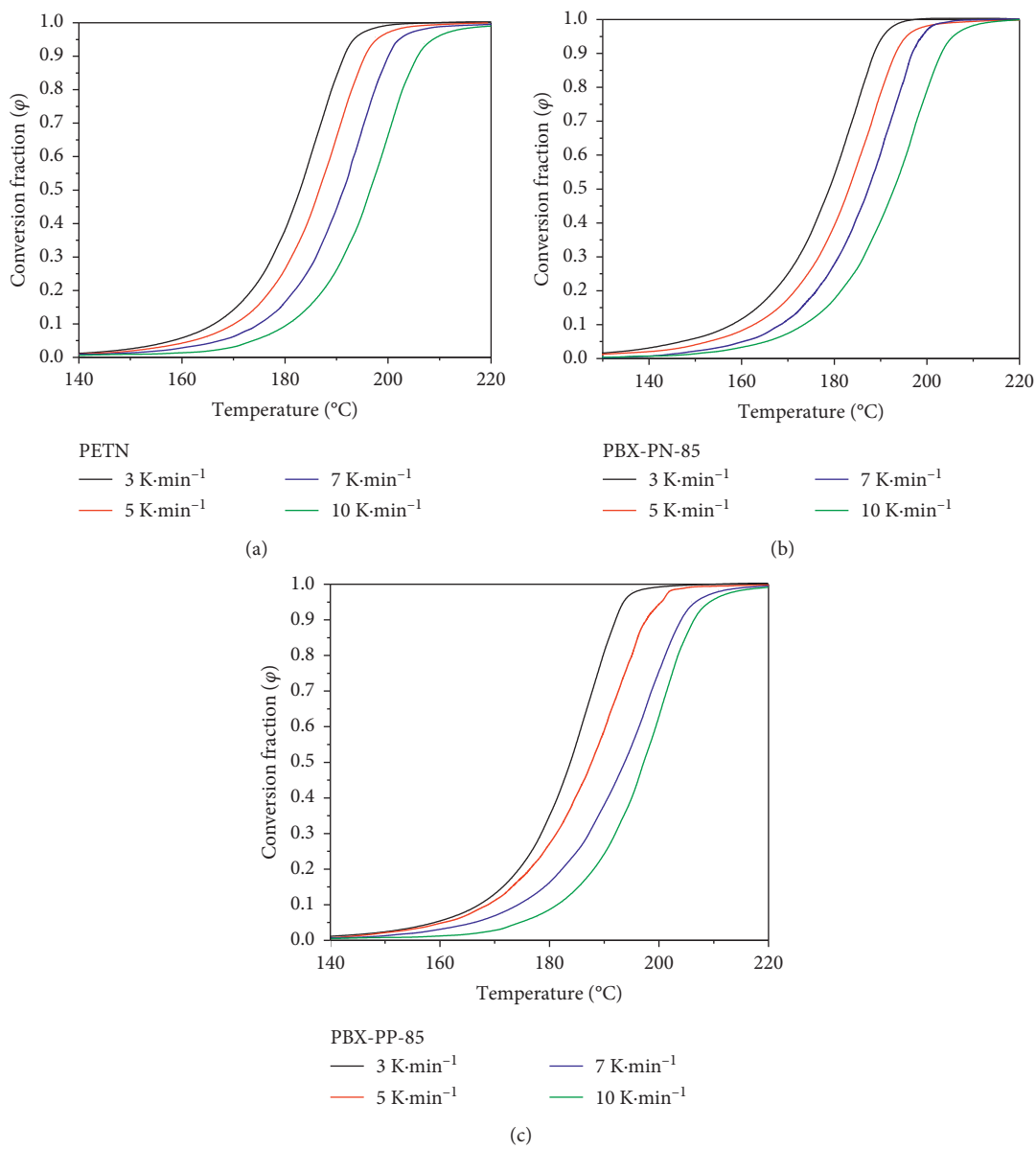

Figure 2: φ versus T curves of PETN, PBX-PN-85, and PBX-PP-85 at several heating rates.

presented in Figure 2. It can be observed that all of the $\varphi - T$ curves have the form of the sigmoid function (i.e., the "S" shape curve), which is often obtained in the thermal analysis of high energetic material [29].

As recommended by the ICTAC kinetics committee [21, 30], the modified Kissinger–Akahira–Sunose (KAS) technique was applied for investigating the relationship between the activation energy and the conversion fraction. The fitting lines at each conversion fraction are presented in Figure 3 by plotting $\ln(\beta/T^2)$ against $1/T$.

The activation energy E_φ and the pre-exponential factor A of the thermal decomposition of all samples were evaluated based on the slopes and intercepts of the plots shown in Figure 3 and are expressed in Table 4. The dependence of activation energy on the conversion by the modified KAS method is shown in Figure 4.

The mean activation energy (E_φ) values (calculated according to the modified KAS method with the conversion range of 0.3–0.7 [13, 16]) of single PETN, PBX-PN-85, and PBX-PP-85 are 144.9, 137.1, and 152.4 kJ·mol^{-1}, respectively.

To verify these results obtained by the KAS method, the kinetic parameters were recalculated using NETZSCH Thermokinetic software according to the ASTM E698 [31]. The E_φ values of single PETN, PBX-PN-85, and PBX-PP-85 are 138.2, 129.7, and 150.9 kJ·mol^{-1}, respectively. The results were close to those obtained from the KAS method with the maximum difference of approximately 5%, which indicates the accuracy and reliability of measurements.

Compared to single PETN, the introduction of NC in PBX-PN-85 formulation leads to the decrease of its

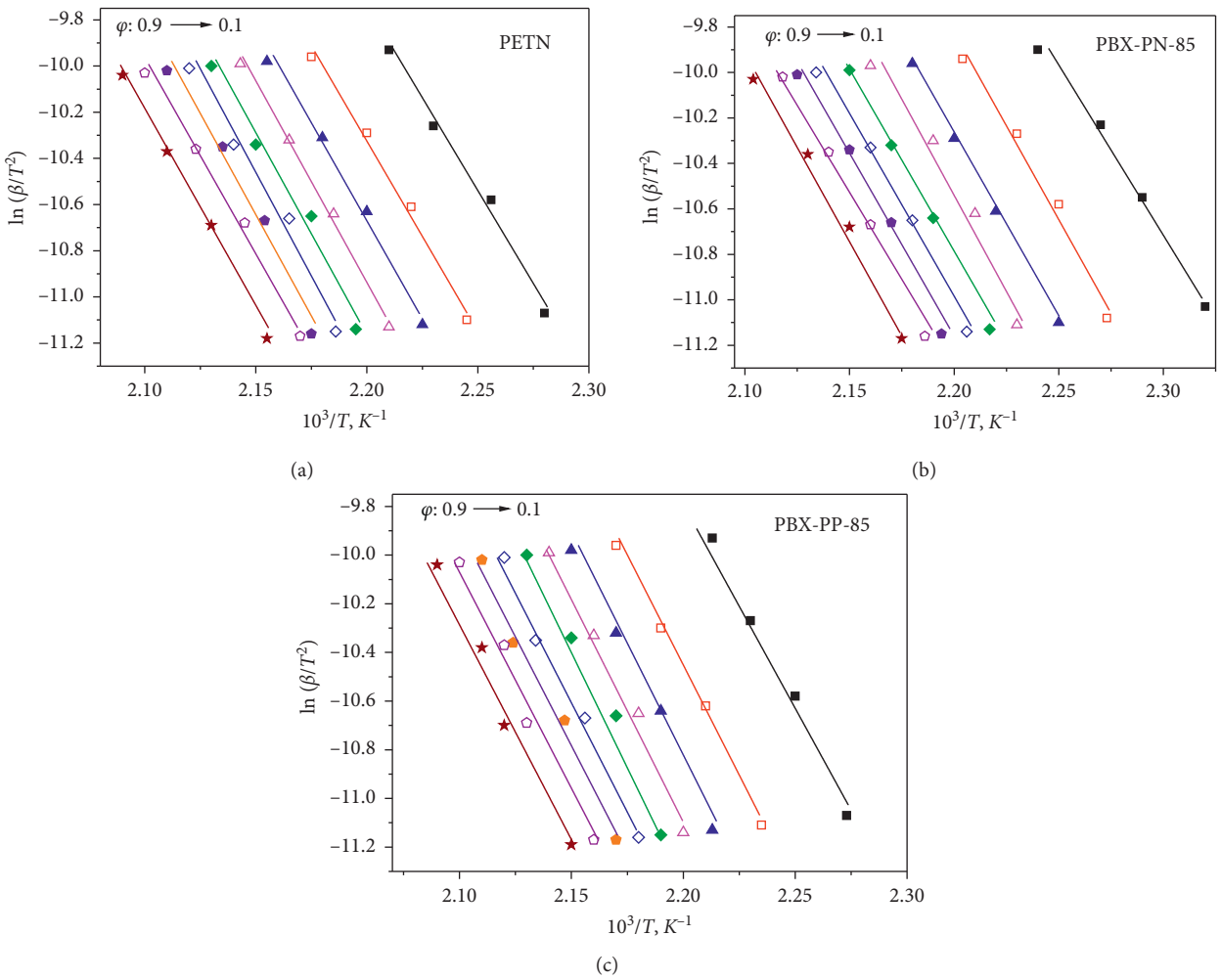

Figure 3: Isoconversional plots at selected conversion degree of PETN, PBX-PN-85, and PBX-PP-85 according to the modified KAS method.

Table 4: Kinetic parameters of PETN and PBXs by the modified KAS method.

φ	PETN			PBX-PN-85			PBX-PP-85		
	E_φ (kJ·mol^{-1})	ln A, (min^{-1})	R^2	E_φ (kJ·mol^{-1})	ln A, (min^{-1})	R^2	E_φ (kJ·mol^{-1})	ln A, (min^{-1})	R^2
0.1	133.8	24.7	0.9955	124.5	21.3	0.9835	139.3	27.8	0.9880
0.2	138.3	26.3	0.9915	136.3	25.4	0.9905	150.4	32.5	0.9950
0.3	141.3	27.2	0.9850	136.5	24.9	0.9945	152.6	33.2	0.9915
0.4	145.2	28.4	0.9884	138.6	26.8	0.9964	152.1	32.4	0.9835
0.5	145.3	28.6	0.9935	137.9	24.8	0.9924	155.5	34.1	0.9980
0.6	147.1	29.9	0.9828	136.6	24.6	0.9920	153.2	32.2	0.9909
0.7	145.8	28.9	0.9845	135.8	24.7	0.9960	148.5	31.3	0.9945
0.8	141.4	27.5	0.9899	137.9	26.4	0.9949	147.6	29.8	0.9952
0.9	141.8	27.7	0.9854	127.2	22.6	0.9935	146.7	27.8	0.9960
Mean	**144.9**	**28.6**		**137.1**	**25.2**		**152.4**	**32.6**	

activation energy because the thermal stability of the nitrate group in NC is less than that in PETN [32, 33]. For PBX-PP-85 formulation, besides the reducing mechanical sensitivity of the explosive, an inert binder system (i.e., DOP/PS) acts as a stabilizer by trapping the active thermal decomposition product [29, 34], resulting in the higher activation energy and thus higher stability versus single PETN.

3.2. The VST Results. Results of TG/DTG were verified by VST studies, which were conducted at several isothermal temperatures (e.g., 125, 130, 135, and 140°C). From the relationship of the volume of released gas versus heating time in VST tests, the conversion fraction values (φ) for each time (t) were computed according to equation (3), and the curve of the conversion fraction (φ) versus heating time (t) is plotted for all samples in Figure 5.

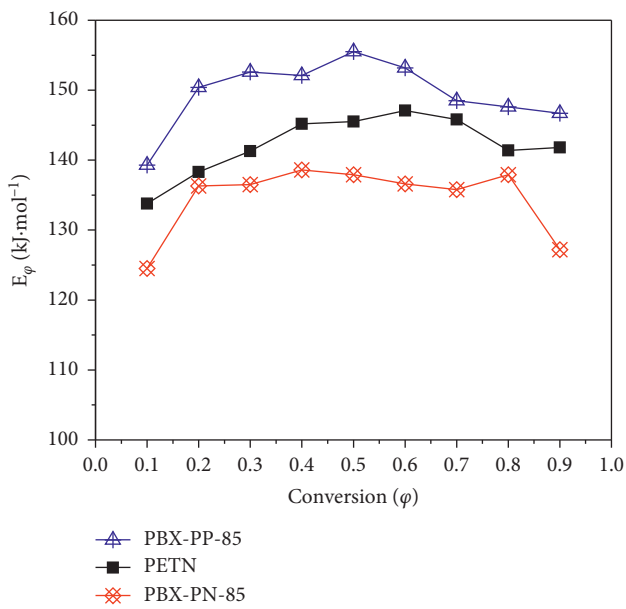

Figure 4: The dependence of activation energy on the conversion by the modified KAS method.

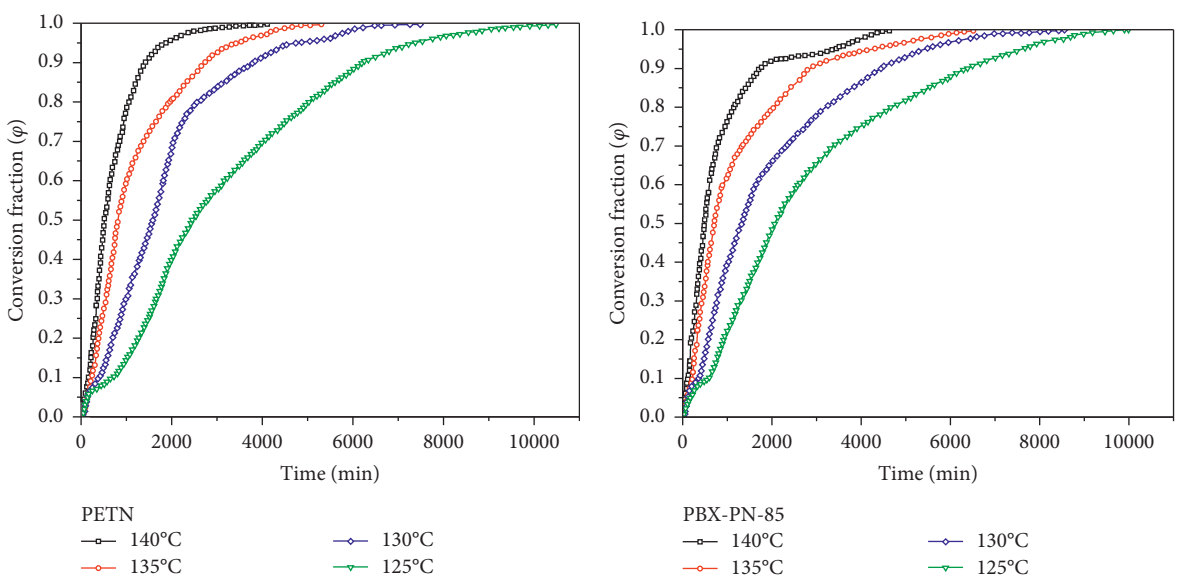

Figure 5: Continued.

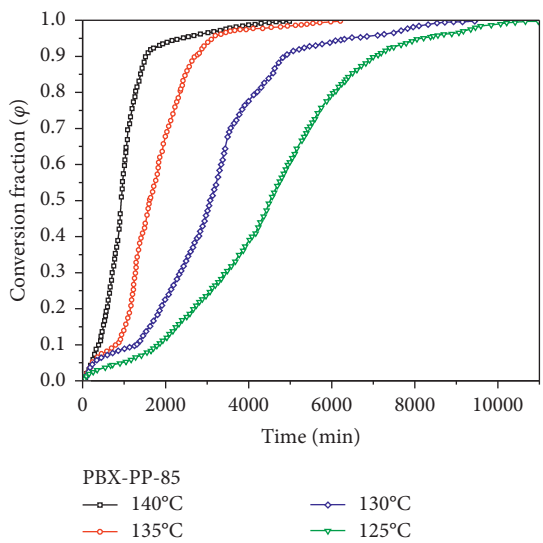

(c)

Figure 5: Conversion fractions (φ) versus heating time t for PBX-PN-85, PBX-PP-85, and PETN.

It is obvious from Figure 5 that the obtained $\varphi - t$ curves of PBX-PN-85, PBX-PP-85, and PETN obey the logarithmic trend, and the decomposition rate of all samples increased when the temperature was increased. In the case of PBX-PN-85 and PETN, it is apparent that the conversion grew rapidly during the first 2000 minutes and the conversion rate is low in the next 8000 minutes until the samples were completely decomposed. Similarly, the conversion rate of PBX-PP-85 can also be derived from Figure 5. In the case of PBX-PP-85, the conversion also increased rapidly in the first 2000 minutes at 135 and 140°C, while the conversion took longer time when tested at 125 and 130°C. By comparing the results of all samples, it was found that PBX-PP-85 sample took a longer time for completing the conversion than PBX-PN-85 and PETN samples. For example, at an isothermal temperature 125°C, the time for completing the conversion of PBX-PN-85, PETN, and PBX-PP-85 was 9990, 10485, and 10970 min, respectively. The differences in the thermal stability of three samples were assessed by the activation energy employing the model-free (isoconversional) and model-fitting methods.

3.2.1. Isothermal Isoconversional Method from VST Data. Next, we utilize VST data to find kinetics parameters of PBX samples. By drawing $-\ln(t)$ versus $1/T$ curve at each temperature according to equation (7) for each conversion φ, the kinetic thermal decomposition parameters of three samples were calculated and are expressed in Table 5. The dependence of activation energy on the conversion is presented in Figure 6.

These E_φ values are in the same range of the E_φ values calculated from TG/DTG data using the modified KAS method, thus demonstrating the reliability of the VST test in evaluating the E_φ values of studied samples by the isothermal isoconversional method. The E_φ values of PETN, PBX-PN-85, and PBX-PP-85 were 137.3, 129.7, and 143.9 kJ·mol^{-1}, respectively. Besides that, the $\ln(A)$ values of PETN, PBX-PN-85, and PBX-PP-85 were 31.9, 28.0, and 35.0 min^{-1}, respectively.

3.2.2. Isothermal Model-Fitting Method from VST Data. The model-fitting method includes two fits: *the first fit* for determination of the model rate constant $k(T)$ that best fits the VST data and *the second fit* for determination of several kinetic parameters such as pre-exponential factor A from the Arrhenius equation and the activation energy E_φ [13, 22]. Fourteen reaction models from Table 1 were selected for fitting the conversion of the thermal decomposition. Table 6 shows the results for the pre-exponential factor, the activation energy, and squares of the correlation coefficients obtained by plotting the integrated form $i(\varphi)$ versus heating time t at each isothermal temperature.

From Table 6, it was observed that the kinetic parameters (specifically, pre-exponential factor and activation energy), which are derived from the VST data utilizing the model-fitting method, are essentially independent of the reaction model used. It means that there is an insignificant difference between the kinetic parameters (i.e., E_φ and A) calculated using different model reactions. For selecting the best model fitting, the correlation coefficient R^2 was used as a parameter. It was found that the best model that describes the thermal decomposition of PETN is contracting volume (R3) and the best model for PBX-PN-85 is 3-D diffusion-Jander (D3) while the best model for PBX-PP-85 is second-order (F2).

On the other hand, we found that the activation energy values calculated by the isothermal isoconversional method are approximate to those derived from the isothermal model-fitting method using the VST technique. To make a

Table 5: Kinetic parameter of PETN and PBXs by the isothermal isoconversional method.

φ	PETN			PBX-PN-85			PBX-PP-85		
	E_φ (kJ·mol^{-1})	ln A, (min^{-1})	R^2	E_φ (kJ·mol^{-1})	ln A, (min^{-1})	R^2	E_φ (kJ·mol^{-1})	ln A, (min^{-1})	R^2
0.1	130.2	29.4	0.9835	123.9	24.1	0.9966	135.6	31.1	0.9767
0.2	137.4	31.8	0.9830	127.2	26.3	0.9921	138.4	32.5	0.9773
0.3	137.9	32.0	0.9962	128.6	27.3	0.9938	145.6	34.9	0.9897
0.4	139.2	32.5	0.9949	132.3	28.9	0.9939	147.3	35.7	0.9890
0.5	142.6	33.7	0.9889	132.3	29.2	0.9924	147.9	36.2	0.9883
0.6	143.6	34.0	0.9930	135.9	30.5	0.9967	147.5	36.4	0.9885
0.7	136.8	32.0	0.9854	137.5	31.1	0.9858	145.5	36.1	0.9900
0.8	136.6	31.9	0.9868	128.7	28.6	0.9885	145.3	36.5	0.9857
0.9	131.2	30.2	0.9831	121.4	26.6	0.9941	142.0	36.2	0.9879
Mean	**137.3**	**31.9**		**129.7**	**28.0**		**143.9**	**35.0**	

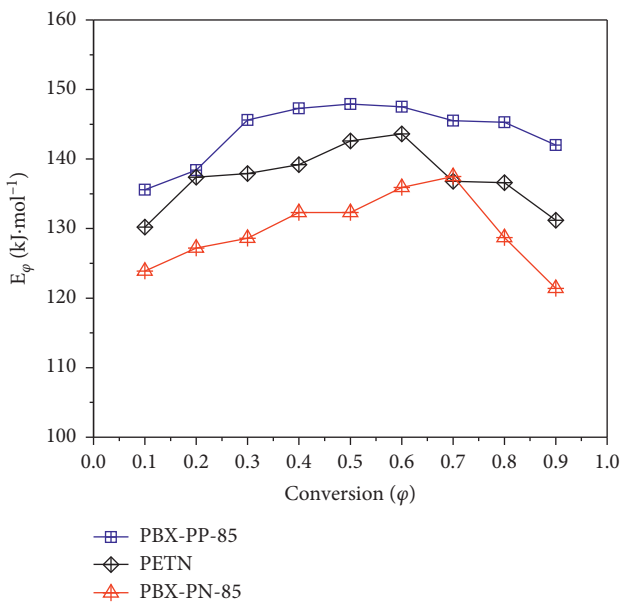

Figure 6: The dependence of activation energy on the conversion using the VST technique.

Table 6: Kinetic parameters of PETN and PBXs calculated from the model-fitting method.

Model	PETN			PBX-PN-85			PBX-PP-85		
	E_φ (kJ mol^{-1})	ln A, (min^{-1})	R^2	E_φ (kJ mol^{-1})	ln A, (min^{-1})	R^2	E_φ (kJ mol^{-1})	ln A, (min^{-1})	R^2
1	137.4	32.4	0.9818	122.0	27.6	0.9828	144.4	34.6	0.9896
2	138.5	32.5	0.9815	121.6	27.2	0.9830	144.5	34.4	0.9896
3	138.3	32.3	0.9827	121.9	27.1	0.9821	144.5	34.0	0.9892
4	139.1	33.6	0.9900	123.5	28.7	0.9846	146.4	35.8	0.9908
5	138.5	33.0	0.9890	122.8	28.2	0.9833	146.2	35.4	0.9907
6	134.1	31.4	0.9845	122.9	27.9	0.9838	146.1	35.1	0.9904
7	139.4	33.0	0.9838	123.9	28.3	0.9853	146.9	35.3	0.9906
8	139.1	32.7	0.9935	123.9	28.1	0.9844	146.9	35.1	0.9908
9	139.4	32.3	0.9862	123.7	28.5	0.9862	147.6	35.8	0.9905
10	139.8	33.3	0.9754	119.7	27.2	0.9855	146.7	35.2	0.9886
11	140.6	32.6	0.9860	125.6	28.0	0.9918	148.5	34.9	0.9913
12	139.7	34.4	0.9853	124.9	29.8	0.9853	148.2	36.6	0.9914
13	141.3	36.2	0.9846	124.8	31.1	0.9846	150.6	36.9	0.9940
14	142.6	38.2	0.9834	129.6	34.2	0.9834	152.4	40.0	0.9903

Table 7: Kinetic parameters of PETN and PBXs obtained by several methods.

Sample	TG/DTG using KAS method		Vacuum stability test (VST)			
			Isoconversional method		Model-fitting method	
	E_φ (kJ·mol^{-1})	ln A (min^{-1})	E_φ (kJ·mol^{-1})	ln A (min^{-1})	E_φ (kJ·mol^{-1})	ln A (min^{-1})
PETN	144.9	28.6	137.3	31.9	139.1	32.7
PBX-PN-85	137.1	25.2	129.7	28.0	125.6	28.0
PBX-PP-85	152.4	32.6	143.9	35.0	150.6	36.9

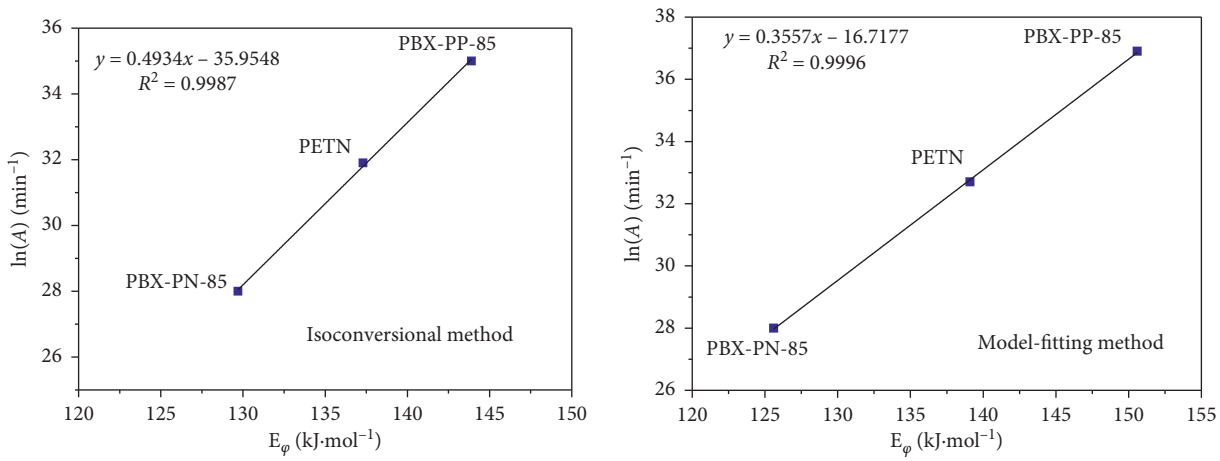

Figure 7: The linear dependence of E_φ with ln A of all samples obtained from the VST test.

comparison, kinetic parameters obtained by different methods are presented in Table 7.

The values in Table 7 demonstrate the role of the binder on the initiation activation energy of PETN. The energetic binder based on NC reduces the activation energy (i.e., PBX-PN-85 has lower thermal stability than that of PETN), while the introduction of the nonenergetic material based on PS increases the activation energy of the explosive.

The ranges of E_φ values obtained by different methods were 125.6–137.1 kJ·mol^{-1} for PBX-PN-85, 137.3–144.9 kJ·mol^{-1} for PETN, and 143.9–152.4 kJ·mol^{-1} for PBX-PP-85. These ranges are narrow, proving the equivalence of these methods with each other. It is also noteworthy that E_φ of PETN obtained in this work is in good agreement with that reported by Pouretedal et al. [15] (135.1–136.9 kJ·mol^{-1}) and by Künzel et al. [16] (137.4 ± 3.4 kJ·mol^{-1}).

According to Brill et al. [35], the E_φ and ln A values—determined from isothermal techniques in the same conditions—usually compensate each other. They found that all of E_φ – ln A pairs that lie in the regression line represent legitimate measurement and reliable results. We have plotted all E_φ values of PETN, PBX-PN-85, and PBX-PP-85 versus corresponding ln A values (presented in Table 7) in Figure 7.

It can be observed the linear relationship of E_φ with ln A values, which confirm the accuracy of the kinetic parameters obtained by the isoconversional method and model-fitting method using the VST test.

4. Conclusions

The thermal decomposition behavior and kinetics of PETN, PBX-PN-85 (85% PETN, 15% NC-based binder), and PBX-PP-85 (85% PETN, 15% PS-based binder) were examined by TG/DTG and VST techniques using model-fitting and isoconversional methods. The activation energy values computed by the non-isothermal technique (modified KAS method) were close to those calculated by model-fitting and isothermal isoconversional methods, ranging from 125.6–137.1 kJ·mol^{-1} for PBX-PN-85, 137.3–144.9 kJ·mol^{-1} for PETN, and 143.9–152.4 kJ·mol^{-1} for PBX-PP-85. The results indicate that the NC-based binder accelerates the thermal decomposition of PBX, thus reducing the activation energy of single PETN. One more valuable conclusion of this study is the influence of the PS-based binder. Specifically, the presence of the PS-based binder causes no adverse effect on the thermal stability of the main explosive in PBX composition.

Data Availability

The data used to support the findings of this study are included in the article.

Conflicts of Interest

The authors declare that they have no conflicts of interest.

Acknowledgments

DVT gratefully acknowledges the support of Vietnam National Foundation for Science and Technology Development (NAFOSTED) under grant no. 107.02-2018.30.

References

[1] J. P. Agrawal, *High Energy Materials: Propellants, Explosives and Pyrotechnics*, John Wiley & Sons, Hoboken, NJ, USA, 2010.

[2] T. Urbanski, *Chemistry and Technology of Explosives*, vol. 2, Pergamon Press, New York, NY, USA, 1965.

[3] A. Elbeih, J. Pachman, S. Zeman, and Z. Akstein, "Replacement of PETN by bicyclo-HMX in semtex 10. Problem of mechatronic," *Armament, Aviation, Safety Engineering*, vol. 1, pp. 7–16, 2010.

[4] H.-S. Kim and B.-S. Park, "Characteristics of the insensitive pressed plastic bonded explosive, DXD-59," *Propellants, Explosives, Pyrotechnics*, vol. 24, no. 4, pp. 217–220, 1999.

[5] S. Moore, M. Schantz, and W. MacCrehan, "Characterization of three types of semtex (H, 1A, and 10)," *Propellants, Explosives, Pyrotechnics*, vol. 35, no. 6, pp. 540–549, 2010.

[6] A. Elbeih, S. Zeman, M. Jungova, and Z. Akstein, "Effect of different polymeric matrices on the sensitivity and performance of interesting cyclic nitramines," *Central European Journal of Energetic Materials*, vol. 9, no. 2, pp. 131–138, 2012.

[7] A. Elbeih, S. Zeman, and J. Pachman, "Effect of polar plasticizers on the characteristics of selected cyclic nitramines," *Central European Journal of Energetic Materials*, vol. 10, no. 3, pp. 339–350, 2013.

[8] N. T. Toan, P. D. Nhan, and V. H. Phuong, "Thermal decomposition and shelf-life of PETN and PBX based on PETN using thermal methods," *Vietnam Journal of Science and Technology*, vol. 56, no. 3, pp. 303–311, 2018.

[9] A. Elbeih, M. M. Mohamed, and T. Wafy, "Sensitivity and detonation characteristics of selected nitramines bonded by sylgard binder," *Propellants, Explosives, Pyrotechnics*, vol. 41, no. 6, pp. 1044–1049, 2016.

[10] B. Vogelsanger, "Chemical stability, compatibility and shelf life of explosives," *CHIMIA International Journal for Chemistry*, vol. 58, no. 6, pp. 401–408, 2004.

[11] Q.-L. Yan, S. Zeman, and A. Elbeih, "Recent advances in thermal analysis and stability evaluation of insensitive plastic bonded explosives (PBXs)," *Thermochimica Acta*, vol. 537, pp. 1–12, 2012.

[12] Q.-L. Yan, S. Zeman, P. E. Sánchez Jiménez, F.-Q. Zhao, L. A. Pérez-Maqueda, and J. Málek, "The effect of polymer matrices on the thermal hazard properties of RDX-based PBXs by using model-free and combined kinetic analysis," *Journal of Hazardous Materials*, vol. 271, pp. 185–195, 2014.

[13] M. Abd-Elghany, A. Elbeih, and S. Hassanein, "Thermal behavior and decomposition kinetics of RDX and RDX/HTPB composition using various techniques and methods," *Central European Journal of Energetic Materials*, vol. 13, no. 3, pp. 714–735, 2016.

[14] T. Nguyen, D. Phan, D. Nguyen, V. Do, and L. Bach, "The chemical compatibility and adhesion of energetic materials with several polymers and binders: an experimental study," *Polymers*, vol. 10, no. 12, p. 1396, 2018.

[15] H. R. Pouretedal, S. Damiri, M. Ravanbod, M. Haghdost, and S. Masoudi, "The kinetic of thermal decomposition of PETN, Pentastite and Pentolite by TG/DTA non-isothermal methods," *Journal of Thermal Analysis and Calorimetry*, vol. 129, no. 1, pp. 521–529, 2017.

[16] M. Künzel, Q.-L. Yan, J. Šelešovský, S. Zeman, and R. Matyáš, "Thermal behavior and decomposition kinetics of ETN and its mixtures with PETN and RDX," *Journal of Thermal Analysis and Calorimetry*, vol. 115, no. 1, pp. 289–299, 2013.

[17] K.-S. Jaw and J.-S. Lee, "Thermal behaviors of PETN base polymer bonded explosives," *Journal of Thermal Analysis and Calorimetry*, vol. 93, no. 3, pp. 953–957, 2008.

[18] C.-C. Huang, M.-D. Ger, and S.-I. Chen, "Study on thermal decomposition of Pentolites by modified vacuum stability apparatus and differential scanning calorimetry," *Propellants, Explosives, Pyrotechnics*, vol. 17, no. 5, pp. 254–259, 1992.

[19] S. K. Bhattacharia, J. Nunley, and B. L. Weeks, "New insights into kinetics of PETN decomposition from the product and reactant point of view: an investigation with mass spectrometry and differential scanning calorimetry," *Thermochimica Acta*, vol. 617, pp. 38–43, 2015.

[20] W. P. C. De Klerk, M. A. Schrader, and A. C. Van der Steen, "Compatibility testing of energetic materials, which technique?" *Journal of Thermal Analysis and Calorimetry*, vol. 56, no. 3, pp. 1123–1131, 1999.

[21] S. Vyazovkin, A. K. Burnham, J. M. Criado, L. A. Pérez-Maqueda, C. Popescu, and N. Sbirrazzuoli, "ICTAC kinetics committee recommendations for performing kinetic computations on thermal analysis data," *Thermochimica Acta*, vol. 520, no. 1-2, pp. 1–19, 2011.

[22] S. Vyazovkin and C. A. Wight, "Isothermal and non-isothermal kinetics of thermally stimulated reactions of solids," *International Reviews in Physical Chemistry*, vol. 17, no. 3, pp. 407–433, 1998.

[23] Q.-L. Yan, S. Zeman, F.-Q. Zhao, and A. Elbeih, "Nonisothermal analysis of C4 bonded explosives containing different cyclic nitramines," *Thermochimica Acta*, vol. 556, pp. 6–12, 2013.

[24] A. Elbeih, M. Abd-Elghany, and T. Elshenawy, "Application of vacuum stability test to determine thermal decomposition kinetics of nitramines bonded by polyurethane matrix," *Acta Astronautica*, vol. 132, pp. 124–130, 2017.

[25] A. Singh, G. Kaur, C. Sarkar, and N. Mukherjee, "Investigations on chemical, thermal decomposition behavior, kinetics, reaction mechanism and thermodynamic properties of aged TATB," *Central European Journal of Energetic Materials*, vol. 15, no. 2, pp. 258–282, 2018.

[26] H. E. Kissinger, "Variation of peak temperature with heating rate in differential thermal analysis," *Journal of Research of the National Bureau of Standards*, vol. 57, no. 4, pp. 217–221, 1956.

[27] G. I. Senum and R. T. Yang, "Rational approximations of the integral of the Arrhenius function," *Journal of Thermal Analysis*, vol. 11, no. 3, pp. 445–447, 1977.

[28] V. Georgieva, D. Zvezdova, and L. Vlaev, "Non-isothermal kinetics of thermal degradation of chitosan," *Chemistry Central Journal*, vol. 6, no. 1, p. 81, 2012.

[29] Q.-L. Yan, S. Zeman, and A. Elbeih, "Thermal behavior and decomposition kinetics of Viton A bonded explosives containing attractive cyclic nitramines," *Thermochimica Acta*, vol. 562, pp. 56–64, 2013.

[30] Q.-L. Yan, S. Zeman, J. Š mand/Cro, R. Svoboda, and A. Elbeih, "Thermal behavior and decomposition kinetics of Formex-bonded explosives containing different cyclic nitramines," *Journal of Thermal Analysis and Calorimetry*, vol. 111, no. 2, pp. 1419–1430, 2012.

[31] ASTM-E-698-11, *Standard Test Method for Arrhenius Kinetic Constants for Thermally Unstable Materials*, American Society for Testing and Materials Philadelphia, Philadelphia, PA, USA, 1979.

[32] J. Kimura, "Chemiluminescence study on thermal decomposition of nitrate esters (PETN and NC)," *Propellants, Explosives, Pyrotechnics*, vol. 14, no. 3, pp. 89–92, 1989.

[33] C.-C. Huang, M.-D. Ger, Y.-C. Lin, and Sun-IChen, "Thermal decomposition of mixtures containing nitrocellulose and pentaerythritol tetranitrate," *Thermochimica Acta*, vol. 208, pp. 147–160, 1992.

[34] N. P. Loginov and S. N. Surkova, "Effectiveness of the action of stabilizers in explosive compositions under mechanical loading," *Combustion, Explosion, and Shock Waves*, vol. 42, no. 1, p. 100, 2006.

[35] T. B. Brill, P. E. Gongwer, and G. K. Williams, "Thermal decomposition of energetic materials. 66. Kinetic compensation effects in HMX, RDX, and NTO," *The Journal of Physical Chemistry*, vol. 98, no. 47, pp. 12242–12247, 1994.

Hindawi
Advances in Materials Science and Engineering
Volume 2020, Article ID 9565394, 10 pages
https://doi.org/10.1155/2020/9565394

Research Article

Design Proposal of a Prototype for Sawdust Pellet Manufacturing through Simulation

J. C. Paredes-Rojas,[1,2] C. R. Torres San Miguel,[3] A. I. Flores Vela,[1,2] B. Bravo-Díaz,[1,2] C. De la Cruz Alejo,[2] and D. Palma Ramírez[1]

[1]*Instituto Politécnico Nacional, Centro Mexicano para la Producción Más Limpia (CMPL), Av. Acueducto S/N, La Laguna Ticomán, 07340 Mexico City, Mexico*
[2]*Instituto Politécnico Nacional, Laboratorio Nacional de Desarrollo y Aseguramiento de la Calidad en Biocombustibles (LANDACBIO), Centro Mexicano para la Producción más Limpia, Av. Acueducto de Guadalupe S/N, La Laguna Ticomán, 07340 Ciudad de México, Mexico*
[3]*Instituto Politécnico Nacional, Escuela Superior de Ingeniería Mecánica y Eléctrica, Sección de Estudios de Posgrado e Investigación, Unidad Profesional "Adolfo López Mateos", Edificio 5 Tercer Piso, Del. Gustavo A. Madero, Col. Lindavista, 07738 Mexico City,, Mexico*

Correspondence should be addressed to J. C. Paredes-Rojas; paredesrojasjc@gmail.com

Received 6 September 2019; Accepted 6 January 2020; Published 12 March 2020

Guest Editor: Costica Bejinariu

Mexican industry generates tons of organic wastes that are not used and cause social, environmental, and health problems. The main organic residue which is generated during wood production is the sawdust (biomass). In order to reduce the problems generated by its waste, a prototype to manufacture biofuel pellets was designed by considering a flat die pelletizing machine according to the standard EN 14961-2. The machine design consists of stainless steel 304 and carbon steel to produce pellets of 6 mm and 30 mm in diameter and length, respectively, at 50–100 rpm. The matrix types proposed were radial, spiral, and hexagonal. In order to be constructed quickly, the design is standardized. Results from finite-element analysis indicate that it is possible to manufacture pellets from 50 to 1000 PSI (344.7 kPa to 6894.7 kPa) with this design complying with the standard.

1. Introduction

The use of fossil fuels as primary energy source has led to a negative impact on the environment such as the global warming and air pollution. Worldwide efforts are being made to produce different technologies based on environmentally-friendly energy production in the last years [1, 2].

Currently, the industry in Mexico has shown interest in substituting fossil fuels by those renewable energy sources [3]. Specifically, the sawmill industry generates a huge amount of waste that complicates the management in parts of the country. Based on this demand, one of the most important alternatives for the development of new products is its biomass [4]. In order to reduce this problem, biofuel pellets from sawdust are a new source of energy, which can be of different types such as briquettes, pales, cubes, wood chips, and pellets [5]. Moreover, beside biofuel, the pellet can be used even for more advance purposes including organic pellet fertilizer production following a composting period and specific procedure [6, 7]. The process to obtain the pellets consists in the collection of raw material, drying, grinding, conditioning, pelletizing/briquetting, and screening/sieving. For this purpose, two pelletizer types can be found: the flat die roller press and the ring die press [8]. Ring die presses are considered as the optimal technologies for wood-derived pellets [9].

Computer-aided technology offers a favorable route to make use of experimental know-how and guide analysis for novel and efficient technologies that allow a fast, cost-effective,

and automated evaluation of a great number of characteristics that may lead to highly efficient machinery. Experimentally obtained results to formulate the mathematical representations are used either in computer simulation or optimization in further experiments to verify the results and the optimization [10]. In this manner, computer-aided technologies play a significant role in the field of solid biofuel technologies. Modelling and simulation of the components of a pelletizing machine are necessary to understand conceptually the systems [11].

Mexico is a country with a wide variety of renewable biomass resources, the technologies for these purposes are deficient, and palletizing machine used to produce sawdust biofuel is topics just emerging [12].

This research is focused on the design and analysis of a flat die compaction machine to produce pellets from sawdust biomass. The roller section as well as the flat die were selected to determine the final parameters to create and set up the geometry of the pelletizer. Then, the main aim of this work was to design and compare the radial, spiral, and hexagonal matrixes to simulate a better pellet production through finite-element analysis. The paper is organized as follows. In Section 2, recent studies are reported in this section. Section 3 describes the technical specifications for pellets machine design and pellets characteristics on standard EN 14961-2. Section 4 shows the main components of the pellets machine, sawdust pressed in a heat-cold press machine, pellet dimensions, sawdust compression, displacement, and safety factor. Section 5 presents conclusions and future work.

2. State of the Art

A utility model described in CN200945426Y (Chinese) consists of a wood processing equipment, where at least two rotatable rollers oppositely arranged on a driving shaft along the axial direction and a roller ring module peripherally arranged. Similarly, the invention in RU2566692C2 (Russian) describes a press granulator for making particles with modular construction and operation with the aim of being adjusted while avoiding the maintenance of the individual modules. In the U.S. Pat. No. 4,511,321, a machine for densifying and pelleting extrudable material is described. It includes, in combination, a flat horizontal die plate and pressure exerting means overlying the die plate, the pressure exerting means having various alternative forms such as a continuous chain means carrying a plurality of spaced pressure members or a reciprocating frame carrying roller means. The CN205672878U relates to a ring die granulator and a granulating device to provide a simple structure, small volume, high efficiency, and low energy consumption of the ring mold in the machine. Another utility model is a circular die granulator with a vertical main shaft equipped with a double reduction machine which drives the main shaft and rotates (CN205517625U). As it was stated by Celik et al., the research related to the design of an optimum die by means of computer-aided engineering and structural optimization approaches is very limited [13]. For this design, parameters such as the force required for densification, the capacity, plugger pressure surface, diameter and hydraulic cylinder speed, densifier flow rate, hydraulic pump, and motor selection were considered. This machine operates without extrusion, preheating chambers, and ejection problems which were associated with the manual press.

Recently, researchers are using Solidworks® software and FEA tool to simulate machine elements, such as the die [14]. For example, the pressure supported by the hydraulic cylinder in a designed compaction machine is of 100 ton at 10,000 PSI (100 000 kg at 68947.5 kPa), whereby it was necessary to ensure the pressure supported by the rear block, upper block, and compaction matrix as well as the blocker. For this reason, Döring analyzed the maximum tensile, elastic limit, and the security factor of the pieces [15]. On the other hand, Macko group optimized the strength and kinematics of the movement of each component with Solidworks® software in a machine with a capacity of up to 100 kg/h [16]. Celik et al. studied the compression ratio (CR) by using a finite-element analysis (FEA) based on design for sample in single-hole flat die parameters (geometry dimensions) against various compression pressure values [13]. Likewise, Šooš et al. developed, designed, and tested a compacting press (with a protected patented) for the production of pressing biofuels of the optimal shape, almost circular shape [17].

In this same context, the fluid mechanics analysis (CFD) of a pellet machine using Solidworks® Flow Simulation indicated that there exist factors important for the granulation. These factors are mainly associated to the quality; some examples are mentioned here: the raw material, performance of the granulating machine and the course of the granulation process, friction in the matrix, surface and material from which the matrix and press are made of, length and diameter of holes in the matrix, the thickness of the biomass material that is subjected to the pressure of the rollers on the surface of the die—the thickness of the material layer reaching the die holes and compression frequency—and the speed at which the press roll moves. However, the model should be limited to one inlet and one outlet and the construction system should be simplified for calculations [18]. In order to analyze a final product in the spheroid shape of pressed biofuels, the construction design of a compacting machine was performed from the optimization of parameters such as the surface to volume ratio, density, and shape. The results indicated that it is necessary to hold the compacted piece for a certain time under high pressure and temperature [19]. Olawale et al. designed a low cost, small scale, 40 bar hydraulic operated piston briquetting machine with a capacity of 120 briquettes per hour [20].

3. Materials and Methods

This work begins with the search for information related to the different types of pellets machine reported. Also, data corresponding to the sawdust and the type of steel that would be used were obtained from the compilation of several data sheets and articles in the literature. Subsequently, calculations were realized by determining the parameters related to the roller part and the flat die that must have the vertical bed pelletizing machine to compact the biomass and generate the pellets. A previous test was carried out to evaluate if the biomass from sawdust could be pressed at pressures closed to those of the standards and reported. For this objective, the biomass was

Table 1: Physical and technical characteristics of numerical simulation considering three types of matrixes based on AISI 304 stainless steel.

Matrix type Study type	Radial Static analysis	Spiral Static analysis	Hexagonal Static analysis
Avg. element size (fraction of model diameter)	0.1	0.1	0.1
Min. element size (fraction of avg. size)	0.2	0.2	0.2
Grading factor	1.5	1.5	1.5
Density (g/cm^3)	8	8	8
Mass (kg)	7. 00588	6.70891	6.42679
Volume (mm^3)	875735	838614	803348
Yield strength (MPa)	215	215	215
Ultimate tensile strength (MPa)	505	505	505
Young's modulus (GPa)	195	195	195
Poisson's ratio	0.29	0.29	0.29

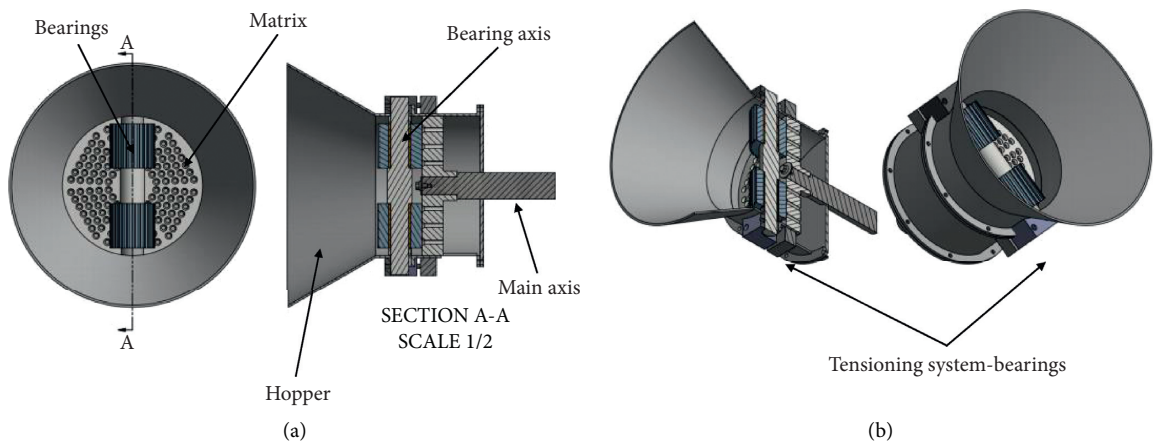

Figure 1: Main components of the pellets machine.

previously dried in an oven at 100°C during 24 h; two types of systems based on particle sizes were considered: the first was as received sawdust and the second was the sawdust milled using a sieve of 0.5 mm in a CT 293 Cyclotec Sample Mill (FOSS, Denmark). A heat-cold press was used to obtain pellets of each particle size. 1 g of product was then pressed under 50, 100, 500, and 1000 PSI (344.7 kPa, 689.4 kPa, 3447.38 kPa, and 6894.7 kPa). Once the data were found and established and after calculating the parameters, Solidworks® software was used to create and edit model geometry of the machine. The machine was designed in carbon steel with the exception of the matrix, which is designed with stainless steel 304 for a production from 300 to 1220 kg/h of a pellet of 6 mm and 300 mm in diameter and length, respectively.

Also, three different matrixes were designed: the radial, spiral, and hexagonal. The radial type is usually used for the pellet production; however, its work surface is not well exploited significantly, whereas designs of the work surface in the spiral and hexagonal types can improve the production of pellets without altering the physical and chemical characteristics of the product. As it is known, the main part is the matrix since it is subjected to stresses and mechanical friction. Thus, the proposed design is needed to be validated by numerical simulation. For this reason, the matrix designs were numerically simulated by using the Software Inventor of Autodesk® version 2017 considering an AISI 304 stainless steel with the physical characteristics seen in Table 1.

Static analysis with a pressure of 8.89476 MPa and 20 MPa in the work surface of the matrix was evaluated. The first value is the type used for this machine and the optimal observed during the physical test in the heat-cold press to obtain the sawdust pellets; however, it is important to mention that a greater pressure was included to corroborate possible strains.

4. Results and Discussion

4.1. Main Components of the Pellet Machine. The modelling obtained from Solidworks® software of the pellets machine is observed in Figure 1, and it is composed by a bearing system of 140 mm and 80 mm in length and diameter, respectively. This system has a bearing connector at the ends adjusted by high-pressure screws; it is important to mention that the bearing has an adjusting guide, which regulates the work pressure. It has a production of 60 kg/h at 50 to 100 rpm of the disk velocity for a pellet with 6 mm and 30 mm in diameter and length, respectively.

4.2. Sawdust Pressed in a Heat-Cold Press Machine. Figure 2 displays the physical aspect of the pellets obtained as primary sawdust and sawdust milled under 50, 100, 500, and 1000 PSI (344.7, 689.4, 3447.38, and 6894.7 kPa, respectively).

It is observed that it is possible to obtain pellets from sawdust biomass either as primary or milled at 0.5 mm of

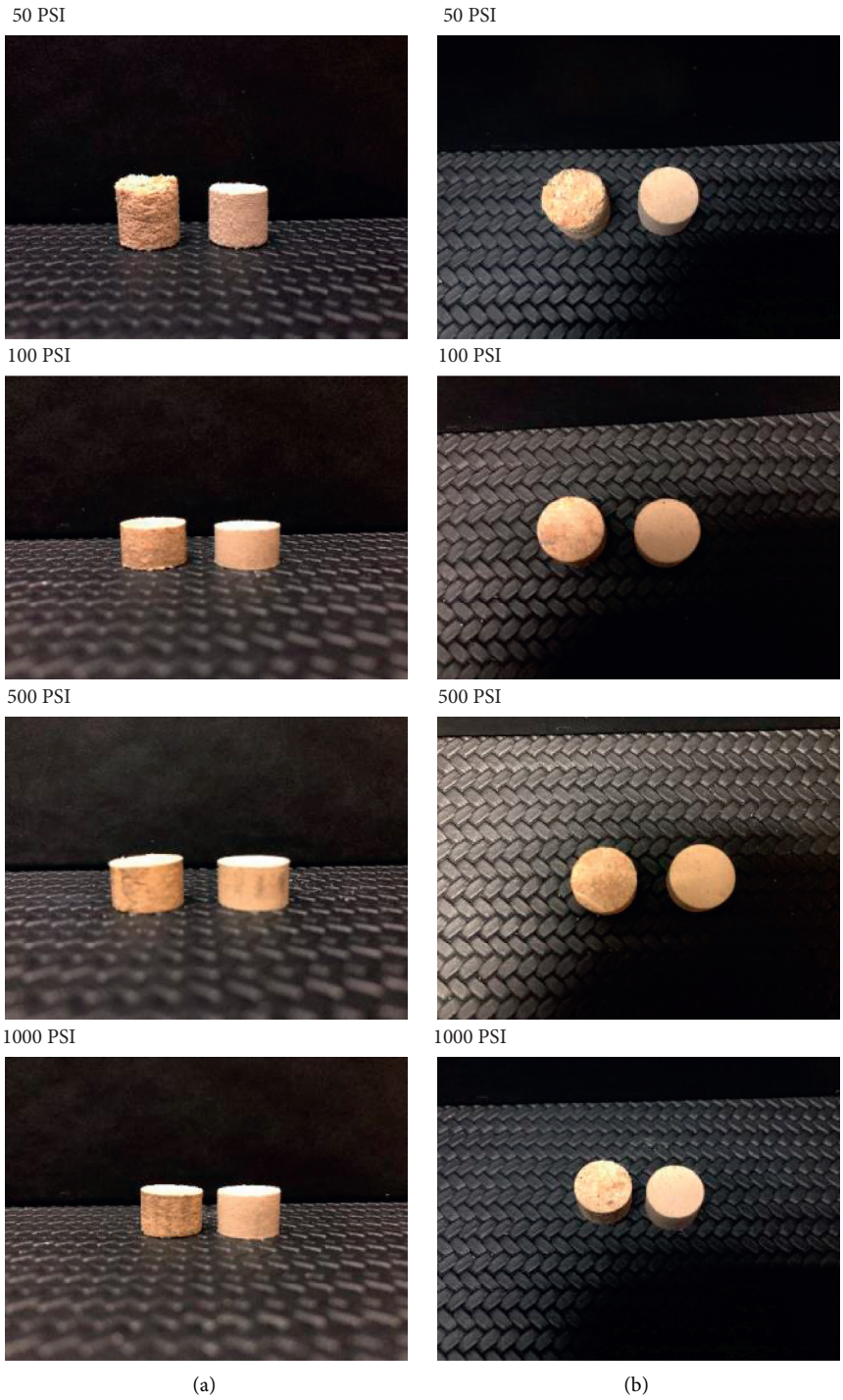

Figure 2: Sawdust pressed under different pressure by using the material as received (a) and milled (b).

particle size. The physical appearance of the pellets improves while increasing the pressure of compacting. For this reason, it was decided and confirmed that 1000 PSI is an optimal condition to use for the machine design.

4.3. Pellet Dimensions. According to the EN-14961-2 and the CEN/TS 14691 standards, a pellet of 6 mm of diameter (Ø) is adequate to avoid the crumbling during transport. For this reason, the pellets studied in this research were selected on the basis of this diameter. The parameters considered for the design of the pelletizing machine are summarized in Table S1 (Supplementary Material). It is important to mention that die pelletizing machine is designed based on the standards EN 14961-2 and CENT/TS 14691, which define the characteristics of the pellet and the certification for solid biofuels, respectively.

4.4. Sawdust Compression. During the compression of sawdust, the rollers have the main function of compressing the

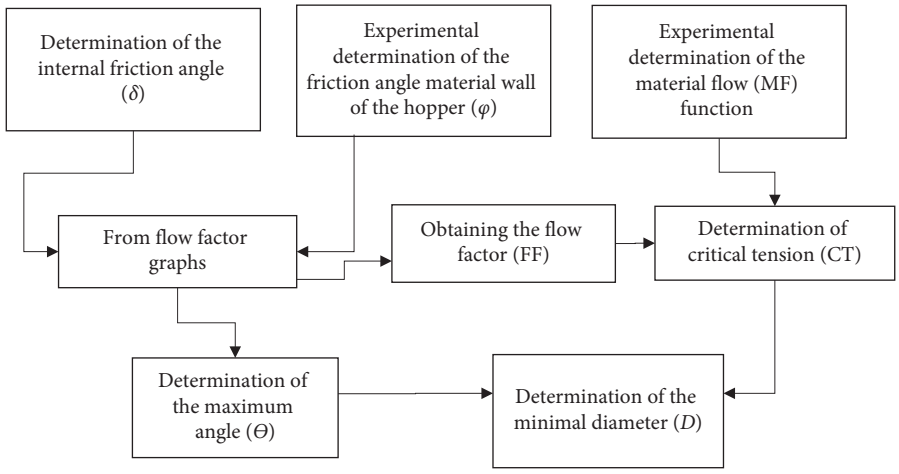

Figure 3: Methodology to determine the hopper data for the design.

material in the hole of the circular flat matrix, and as a consequence, forces are generated in the die. For this reason, different parameters need to be in the account for the compression; they are mentioned in Tables S2–S4 (Supplementary Material).

The power of pelletizer is calculated based on the force required by each roller to press the material at the rotation speed of the main matrix. The worm transmissions are generally used for small and medium power that does not exceed 60 kW. In a small space, they can get the ratio of speed relatively high. For this reason, this type of transmission was selected to give movement to the shaft, which is coupled to the rollers. The worm screws are generally of carbon steel (0.40 to 0.50 wt.% in C) as well as a low alloy steel with Cr and Cr-Ni. The worn of the wheels is manufactured in bronze whose composition depends on the sliding speed and the stress of the transmission (Table S5 Supplementary Material for computation).

The blades are coupled to the main axes, and their rotation speed is of 261 rpm. These blades were considered to be located approximately 5° with respect to the main axis. For the hopper design, the walls with enough steep and low friction were considered. In order to get this goal, the methodology summarized in Figure 3 was used. The results are shown in Table S6 (Supplementary Material for estimation).

For the experimental determination of the material flow (MF) function, the yield stress (Y_{s_cs}) of the confined sawdust and the main stress (σ_1) were considered to construct σ_1 versus Y_s and σ_1 versus $1/Y_s$ plots (see Table 2 and Figure 4). From these plots, the intercept of both straight lines showed the critical tension (CAS), which in this case was c.a. 2 kPa. By using the CAS and (1) and (2), the minimal diameter (D_{minimal}) can be found ($D_{\text{minimal}} = 0.88$ m):

$$H(\theta) = 2 + \frac{\theta}{60^\circ}, \tag{1}$$

$$B = \frac{H(\theta)(\text{CAS})}{\rho g}. \tag{2}$$

The requirement for this machine is 1 L in volume, and for this reason, the height (h_{hopper}) and the diameter

Table 2: Data corresponding to the yield stress of confined sawdust (Y_{s_cs}) and the main stress (σ_1).

σ_1 (kPa)	Y_s (kPa)
5	2.23
10	3.16
20	4.47
44	12
100	8
140	30

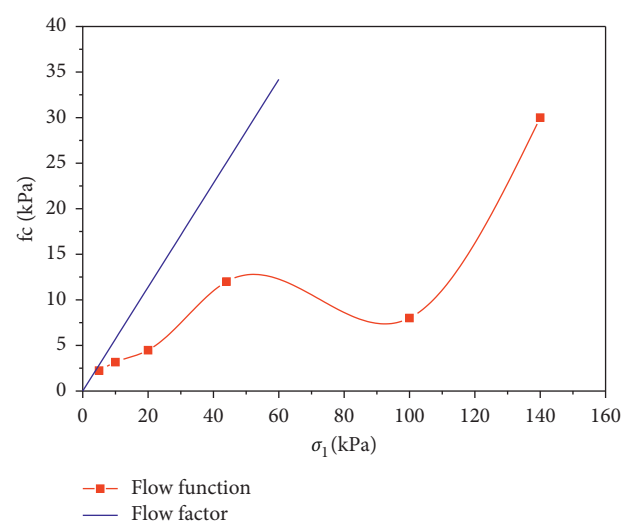

Figure 4: Material flow function (MF) and flow factor (FF) graphs.

(D_{hopper}) of the hopper were assessed on basis of the following equations:

$$V = \frac{\pi}{24\tan(\theta)}\left(D^3 - B^3\right) + \frac{\pi}{4}D_{\text{hopper}}^2 h,$$
$$1 < \frac{H}{D} < 2. \tag{3}$$

Considering $(h/D) = 1$,

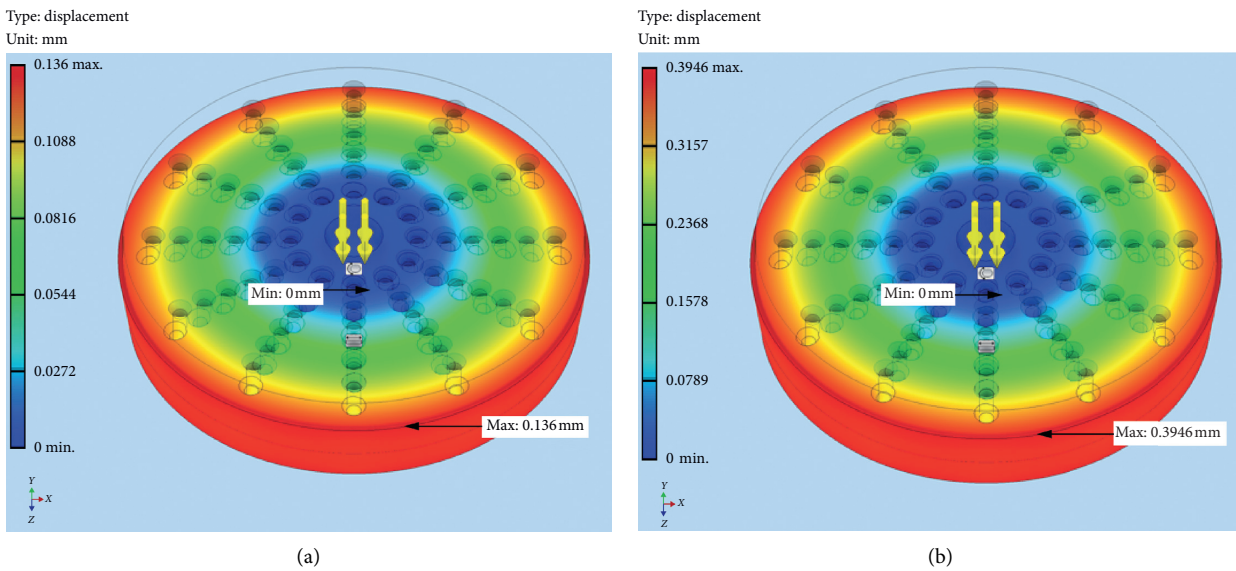

(a) (b)

Figure 5: Static analysis of radial matrix at (a) 1000 PSI and (b) 2900 PSI (6894.7 kPa and 19994.8 kPa, respectively).

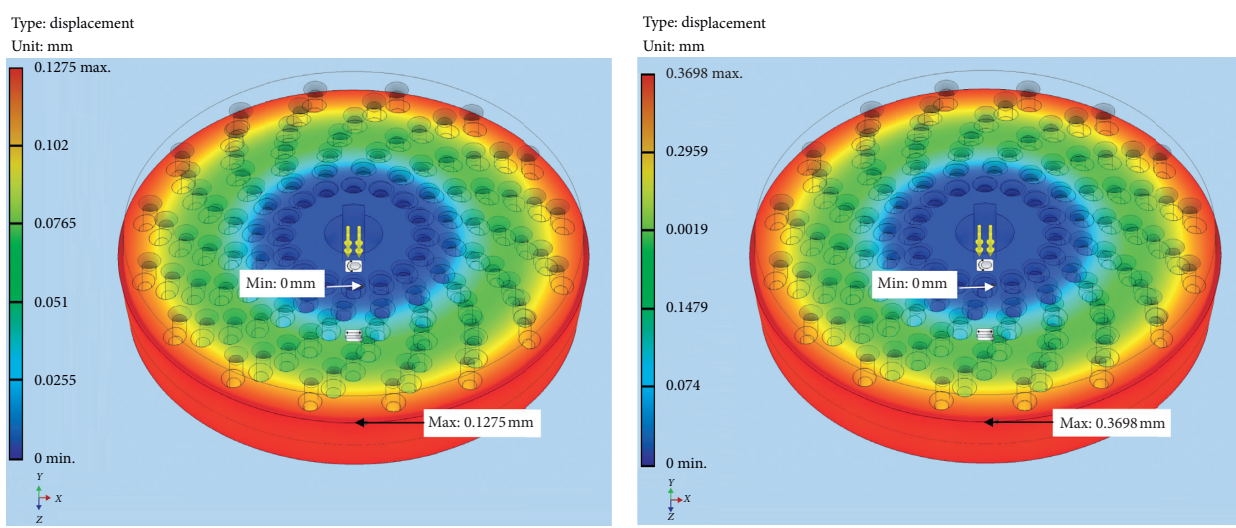

(a) (b)

Figure 6: Static analysis of spiral matrix at (a) 1000 PSI and (b) 2900 PSI (6894.7 kPa and 19994.8 kPa, respectively).

$$h_o = \frac{(D/2)}{\tan\theta} = 2.1494\text{m},$$
$$h_B = \frac{(B/2)}{\tan\theta} = 1.8355, \quad (4)$$
$$h_{\text{hopper}} = h_0 - h_B.$$

D_{hopper} and h_{hopper} correspond to 1.0305 m and 0.3139 m, respectively.

4.5. Displacement. The maximum displacements that pressure can generate in the radial matrix were detected at 0.136 mm and 0.3946 mm at 1000 PSI and 2900 PSI (6894.7 kPa and 19994.8 kPa), respectively. This can be seen in Figure 5. For spiral matrix, the displacement was 0.1275 mm and 0.3698 mm at 1000 PSI and 2900 PSI (6894.7 kPa and 19994.8 kPa), respectively (see Figure 6). And, for the hexagonal matrix, this displacement was 0.1134 mm and 0.3289 mm at 1000 PSI and 2900 PSI (6894.7 kPa and 19994.8 kPa), respectively (see Figure 7).

In this sense, the FEA analysis showed that the three-matrix designs under a pressure of 1000 PSI and 2900 PSI (6894.7 kPa and 19994.8 kPa) are not affected in their mechanical structure since displacement value for the radial disk is 0.3946 and for the hexagonal disk is 0.3289 under a pressure of 2900 PSI (19994.8 kPa).

The static analysis demonstrates that the geometry is a key factor in the matrix design; the hexagonal matrix generates more pellet production in a ratio of 150/72 than that of the

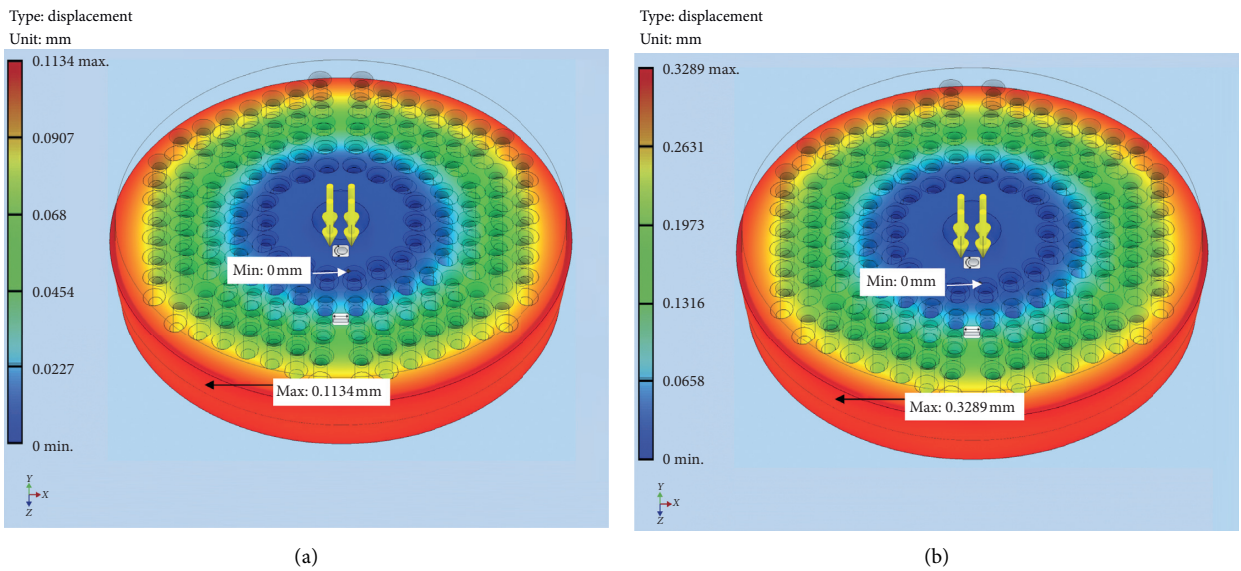

(a) (b)

Figure 7: Static analysis of hexagonal matrix at (a) 1000 PSI and (b) 2900 PSI (6894.7 kPa and 19994.8 kPa, respectively).

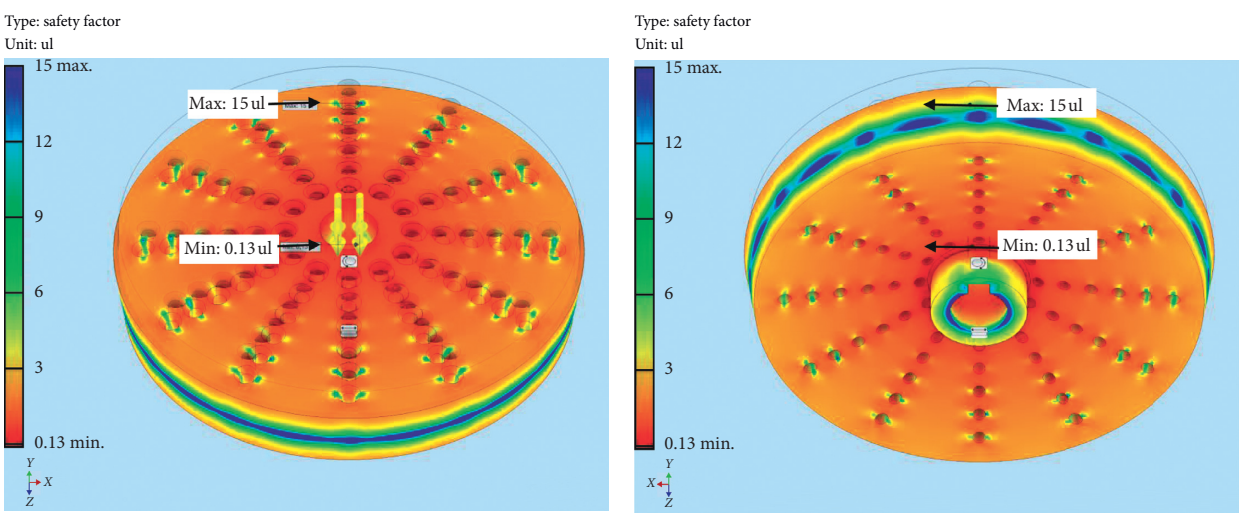

(a) (b)

Figure 8: Safety factor from static analysis of radial matrix at (a) 1000 PSI and (b) 2900 PSI (6894.7 kPa and 19994.8 kPa, respectively).

hexagonal and radial; that is, in comparison to the radial matrix, it is possible to double the production with the configuration of the hexagonal matrix, without affecting its structure.

4.6. Safety Factor. The safety factor is the quotient between the value and the maximum capacity of the system and the value of the actually expected requirement to which it will be subjected; in other words, it indicates the excess of capacity that the system has over its requirements. Figures 8–10 depict the results of the simulation of the three types of matrixes. The safety values were as follows: 0.38 and 0.13 for radial at 1000 and 2900 PSI (6894.7 kPa and 19994.8 kPa), 0.47 and 0.16 for spiral at 1000 and 2900 PSI (6894.7 kPa and 19994.8 kPa), and 0.55 and 0.19 for hexagonal at 1000 and 2900 PSI (6894.7 kPa and 19994.8 kPa).

From these results, a flat die type-pelletizing machine was designed based on the European standard EN 14961-2. Results from FEA simulation showed that the design of the radial, spiral, and hexagonal matrices under a load of 1000 PSI and 2900 PSI (6894.7 kPa and 19994.8 kPa, respectively) is not affected in their mechanical structure. The maximum displacement for radial and hexagonal was 0.3946 mm and 0.3289 mm at a load of 2900 PSI (19994.8 kPa), respectively. These demonstrate that geometry is an important factor during the design; hexagonal matrix will generate more production of pellets in a hexagonal/radial matrix ratio of 150/72. It is possible to double the production with the configuration of the hexagonal

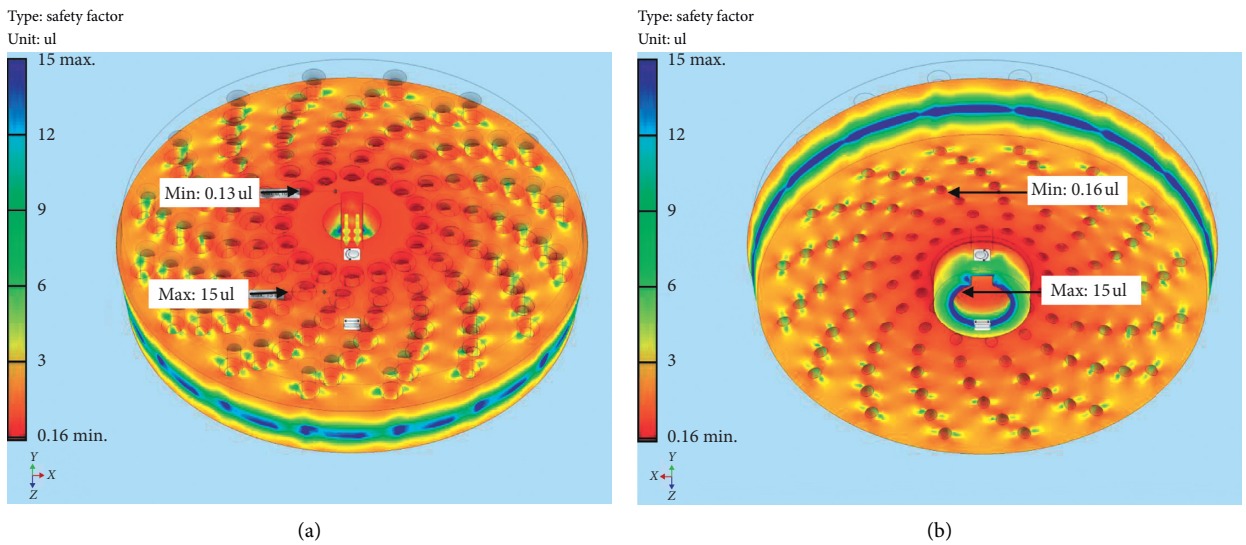

(a) (b)

Figure 9: Safety factor from static analysis of spiral matrix at (a) 1000 PSI and (b) 2900 PSI (6894.7 kPa and 19994.8 kPa, respectively).

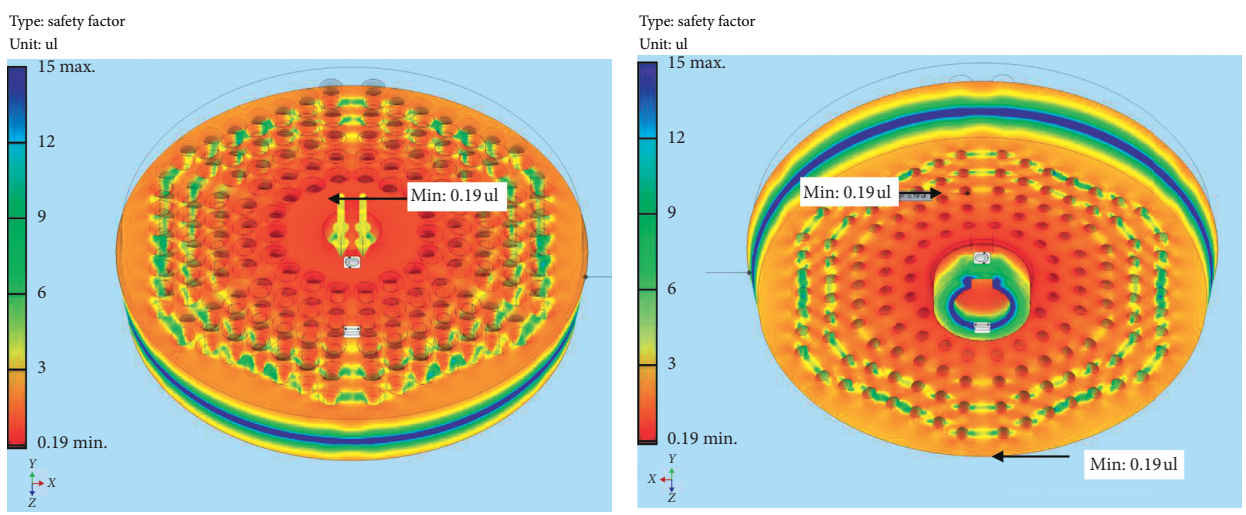

(a) (b)

Figure 10: Safety factor from static analysis of hexagonal matrix at (a) 1000 PSI and (b) 2900 PSI (6894.7 kPa and 19994.8 kPa, respectively).

matrix; this configuration will not affect the structure of the machine. The pellet machine was designed in 304 stainless steel and carbon steel, a production from 300 to 1220 kg/h for a pellet of 6 mm in diameter and 30 mm in length, respectively. The pellet production process is complex because different factors are involved: the type of biomass, humidity, compaction pressure, design and material type of the machine, particle size, sawdust temperature, and matrix speed of rotation.

To support this design, we emphasize on a physical test of compaction, where the pressure, biomass composition, and size particle play a key role. As it is mentioned by Castellano et al. [21], the composition of biomass plays a key role in the quality of pellets since it has an effect on the amount of friction within the channels matrix and determines the potential for particle agglomeration. Similar research studies the raw materials for the production of pellets: fescue, alfalfa, sorghum, triticale, miscanthus, and willow [22], whereas others study the percentage of relative humidity which is an important factor for the production of pellets [23]. It is important to mention that the biomass is not only applied in energy purposes; Souri et al. have studied the nitrogen release as factor of a plant growth after the production of pellet fertilizers as the added value from cow manure. They mention that a low compact pressure is preferred for these purposes [6, 7].

For the numerical simulation by FEA, the compacting pressure used in this work was of 6.89 MPa and 20 MPa (1000 and 2900 PSI), while for the physical test, four different pressures were considered: 0.344, 0.689, 3.447, and 6.894 MPa (50, 100, 500, and 1000 PSI), respectively.

Different studies related to the theoretical compression pressure justify an interval between 188 MPa and 295 MPa. Also, it is mentioned that the biomass, temperature, humidity, and particle size are determinant in the compacting pressure [24]. Compacting pressures of 8.65–9.5 MPa have been reported in the pellet production at the pilot scale [25].

There are different models for the design of the pellet machine [26]; however, the results of this finite-element study and the physical compaction tests showed that it is possible to manufacture pellets with this design, complying with EN 14961-2. Another important point is that the machine design is standardized in order to be manufactured quickly and economically.

5. Conclusions

A flat die type-pelletizing machine was designed based on the European standard EN 14961-2 (define the characteristics of the pellet) and the CENT/TS 14691 standard (European Certification for solid biofuels). This machine was designed in stainless steel 304 and carbon steel, a production of 30 to 60 kg/hr for a pellet of 6 mm in diameter and 30 mm in length; three types of matrix were designed: radial, spiral, and hexagonal; these were compared through simulating for better pellet production. The design was validated through the finite-element method at the three types of matrix and physical compaction tests were performed at different pressures: 50, 100, 500, and 1000 PSI (344.7, 689.4, 3447.38, and 6894.7 kPa).

The results of the simulation by finite elements show that the designs of the matrixes, radial, spiral, and hexagonal, under a load of 1000 PSI and 2900 PSI (6894.7 kPa and 19994.8 kPa), are not affected in their mechanical structure; the static analysis shows that the geometry is an important factor in the design of the matrixes and the hexagonal matrix generates more production of pellets in a ratio of 2 : 1 compared to the radial type, while physical compaction tests show the manufacture of pellets with pressures around of 1000 PSI.

The pellet production process is complex because different factors are involved such as type of biomass, humidity, compaction pressure, design and material type of the machine, particle size, sawdust temperature, and speed of rotation of the matrix between others. For this reason, this work will continue to produce different pellets with different physicochemical parameters and to analyze how those parameters affect the quality of the pellets. The design of this machine is technically standardized in order to be built quickly and economically; however, its construction is necessary to carry out the corresponding tests by taking into account all the factors that can affect the production of the pellets.

Nomenclature

P_{roller}:	Pressure of roller
$\mp$:	Yield stress average during strain
$\in x$:	Strain extrusion
$a = 0.8–0.9$ and $b = 1.2–1.5$:	Empirical constants at an angle between 50° and 60°
A_{die}:	Die surface
Y_s:	The yield stress average of specifically the sawdust during the strain (60 MPa)
h_f:	The initial height after going through the work surface of the roller
P_O:	The pressure of the compressed material against the container wall
μ:	The friction coefficient between the sawdust and the steel
h_0:	The initial height of the material before going through the work surface
D_{roller}:	The diameter of the compacting roller
r_{roller}:	The radius of the compacting roller
a_{roller}:	The surface of the roller
$\rho_{stainless}$:	Density of steel
nv_{roller}:	The normal velocity of the roller
R:	Matrix radius
Q:	Volumetric flow.

Data Availability

The data used to support the findings of this study are available from the corresponding author upon request.

Conflicts of Interest

The authors declare that there are no conflicts of interest regarding the publication of this paper.

Acknowledgments

The authors acknowledge the financial support provided by the Secretaría de Investigación y Posgrado (SIP) of Instituto Politécnico Nacional (IPN) México through the SIP 20192030, 20190040, and 20196710 Projects.

Supplementary Materials

Table S1: pellet main parameters and their corresponding values. Table S2: formula and data of parameters related to the sawdust compression in the die. Table S3: formula and data of parameters related to the roller. Table S4: formula and data of parameters related to the matrix and work surface. Table S5: formula and data related to the required power, the screw, and crown. Table S6: formula and data related to the hopper design. (*Supplementary Materials*)

References

[1] W. Czekała, S. Bartnikowska, J. Dach et al., "The energy value and economic efficiency of solid biofuels produced from digestate and sawdust," *Energy*, vol. 159, pp. 1118–1122, 2018.

[2] F. Martins, C. Felgueiras, M. Smitkova, and N. Caetano, "Analysis of fossil fuel energy consumption and environmental impacts in European countries," *Energies*, vol. 12, no. 6, p. 964, 2019.

[3] D. M. Nikolaevich, F. E. Evgenevna, P. O. Vadimirovna, M. A. Alievich, and O. S. Valerievich, "Study of innovative technologies in the energy industry: nontraditional and renewable energy sources," *Entrepreneurship and Sustainability Issues*, vol. 6, no. 4, pp. 1704–1713, 2019.

[4] D. Hernández, H. Fernández-Puratich, R. Rebolledo-Leiva, C. Tenreiro, and D. Gabriel, "Evaluation of sustainable manufacturing of pellets combining wastes from olive oil and forestry industries," *Industrial Crops and Products*, vol. 134, pp. 338–346, 2019.

[5] I. M. Ríos-Badrán, I. Luzardo-Ocampo, J. F. García-Trejo, J. Santos-Cruz, and C. Gutiérrez-Antonio, "Production and characterization of fuel pellets from rice husk and wheat straw," *Renewable Energy*, vol. 145, pp. 500–507, 2020.

[6] M. K. Souri, M. Rashidi, and M. H. Kianmehr, "Effects of manure-based urea pellets on growth, yield, and nitrate content in coriander, garden cress, and parsley plants," *Journal of Plant Nutrition*, vol. 41, no. 11, pp. 1405–1413, 2018.

[7] M. K. Souri, M. Naiji, and M. H. Kianmehr, "Nitrogen release dynamics of a slow release urea pellet and its effect on growth, yield, and nutrient uptake of sweet basil (*Ocimum basilicum* L.)," *Journal of Plant Nutrition*, vol. 42, no. 6, pp. 604–614, 2019.

[8] W. Stelte, A. R. Sanadi, L. Shang, J. K. Holm, J. Ahrenfeldt, and U. B. Henriksen, "Recent developments in biomass pelletization–a review," *Bioresources*, vol. 7, no. 3, p. 40, 2012.

[9] M. Klemm, R. Schmersahl, C. Kirsten et al., "Upgraded "new" solid biofuels," in *Energy from Organic Materials (Biomass): A Volume in the Encyclopedia of Sustainability Science and Technology*, M. Kaltschmitt, Ed., pp. 451–481, Springer New York, New York, NY, USA, 2nd edition, 2019.

[10] A. I. Papadopoulos, I. Tsivintzelis, P. Linke, and P. Seferlis, *Computer-Aided Molecular Design: Fundamentals, Methods, and Applications*, Elsevier, Amsterdam, Netherlands, 2018.

[11] P. Pal, R. Kumar, N. Srivastava, and J. Chowdhury, "A visual basic simulation software tool for performance analysis of a membrane-based advanced water treatment plant," *Environmental Science and Pollution Research*, vol. 21, no. 3, pp. 1833–1849, 2014.

[12] R. Tauro, M. Serrano-Medrano, and O. Masera, "Solid biofuels in Mexico: a sustainable alternative to satisfy the increasing demand for heat and power," *Clean Technologies and Environmental Policy*, vol. 20, no. 7, pp. 1527–1539, 2018.

[13] H. K. Celik, H. Yilmaz, A. E. W. Rennie, R. Cinar, and M. Z. Firat, "Determination of the failure susceptibility of a flat die used in biomass pelletizing machines by means of FEA-based design exploration," *Journal of Failure Analysis and Prevention*, vol. 18, no. 5, pp. 1099–1110, 2018.

[14] P. M. Kurowski, *Engineering Analysis with SolidWorks Simulation 2010*, SDC Publications, Mission, KS, USA, 2010.

[15] S. Döring, *Pellet Production, Power from Pellets: Technology and Applications*, Springer, Berlin, Geramny, 2013.

[16] M. Macko and A. Mroziński, *Computer Aided Design of Wood Pellet Machines*, Springer International Publishing, Cham, Switzerland, 2019.

[17] Ľ. Šooš, J. Bábics, J. Beniak, P. Križan, P. Kovač, and M. Matúš, "Design and testing functional model compacting machine for produce new shape biofuels," *IOP Conference Series: Materials Science and Engineering*, vol. 501, Article ID 012008, 2019.

[18] M. Macko and A. Mrozinski, "Work parameters research of wood pellet machine," in *Proceedings of the AIP Conference 2077*, Cesme-Izmir, Turkey, May 2019.

[19] Ľ. Šooš, M. Matúš, J. Beniak, and P. Križan, "Development of the compaction machine for the production of new shapes of pressed biofuels," *IOP Conference Series: Materials Science and Engineering*, vol. 297, Article ID 012008, 2018.

[20] U. D. Olawale, E. A. Ademola, S. Taofeek, I. Nageri, A. Olayemi, and I. Rita, "Development and performance evaluation of A low-cost hydraulic-operated biomass briquetting machine," *Journal of Engineering and Technology*, vol. 3, no. 1, pp. 1–6, 2018.

[21] J. M. Castellano, M. Gómez, M. Fernández, L. S. Esteban, and J. E. Carrasco, "Study on the effects of raw materials composition and pelletization conditions on the quality and properties of pellets obtained from different woody and non woody biomasses," *Fuel*, vol. 139, pp. 629–636, 2015.

[22] M. Puig-Arnavat, L. Shang, Z. Sárossy, J. Ahrenfeldt, and U. B. Henriksen, "From a single pellet press to a bench scale pellet mill—pelletizing six different biomass feedstocks," *Fuel Processing Technology*, vol. 142, pp. 27–33, 2016.

[23] Y. Huang, M. Finell, S. Larsson et al., "Biofuel pellets made at low moisture content—influence of water in the binding mechanism of densified biomass," *Biomass and Bioenergy*, vol. 98, pp. 8–14, 2017.

[24] W. Stelte, J. K. Holm, A. R. Sanadi, S. Barsberg, J. Ahrenfeldt, and U. B. Henriksen, "Fuel pellets from biomass: the importance of the pelletizing pressure and its dependency on the processing conditions," *Fuel*, vol. 90, no. 11, pp. 3285–3290, 2011.

[25] M. Ståhl and J. Berghel, "Energy efficient pilot-scale production of wood fuel pellets made from a raw material mix including sawdust and rapeseed cake," *Biomass and Bioenergy*, vol. 35, no. 12, pp. 4849–4854, 2011.

[26] J. E. Arpi Trujillo and C. S. Calderón Toral, "Diseño de una máquina pelletizadora en base a la disponibilidad de residuos madereros de la ciudad de Cuenca para su aprovechamiento energético," Ingeniero Mecánico, Facultad de Ingenierías, Carrera de Ingeniería Mecánimca, Universidad Politecnica Salesiana, Cuenca, Ecuador, 2010.